Department of Medical Biophysics
Institute of Neuroscience and Physiology
Göteborg University

Mechanism of Action of the Antiarrhythmic Agent AZD7009

Frida Persson

Göteborg 2007

ISBN 978-91-628-7047-8

frida.persson@astrazeneca.com

Mechanism of Action of the Antiarrhythmic Agent AZD7009

Frida Persson

Department of Medical Biophysics, Institute of Neuroscience and Physiology, the Sahlgrenska Academy, Göteborg University, Göteborg, Sweden

Abstract

Atrial fibrillation (AF) is the most common tachyarrhythmia in the adult population and is a major cause of morbidity and mortality. AF can be terminated and sinus rhythm restored by prolonging the action potential duration (APD) and the refractory period. Unfortunately, antiarrhythmic agents that prolong the APD and increase the refractory period via selective inhibition of the rapid delayed rectifier potassium current (IK_r), i.e. class III antiarrhythmic drugs, are associated with an increased risk of the ventricular tachycardia Torsades de Pointes. AZD7009 is an antiarrhythmic agent with predominant actions on atrial electrophysiology that shows high antiarrhythmic efficacy and low proarrhythmic potential in animals and man. The aim of the current studies was to characterize the effect of AZD7009 on cardiac ion currents and APD in order to provide a mechanistic explanation for its predominant atrial effects and low proarrhythmic potential.

The human cardiac ion channels hERG (IK_r), Kv1.5 (IK_{ur}), Kv4.3/KChIP2.2 (I_{to}), KvLQT1/minK (IK_s), Kir3.1/Kir3.4 (IK_{ACh}) and Nav1.5 (INa) were expressed in mammalian cells. Whole-cell currents were inhibited by AZD7009 with the following IC_{50} values: hERG 0.6 μM, Nav1.5 8 μM, Kv4.3/KChIP2.2 24 μM, Kv1.5 27 μM, Kir3.1/Kir3.4 166 μM and KvLQT1/minK 193 μM. Whole-cell sodium and calcium currents were recorded in isolated rabbit atrial and ventricular myocytes using amphotericin B perforated patch. The late sodium current in rabbit atrial and ventricular myocytes was inhibited by AZD7009 in a concentration dependent way, with approximately 50% inhibition at 10 μM AZD7009. The L-type Ca^{2+} current (ICa_L) in rabbit ventricular myocytes was inhibited with an IC_{50} of 90 μM. Transmembrane action potentials were recorded in tissue pieces from rabbit atrium, ventricle and Purkinje fibre in control, during exposure to the selective IK_r blocker E-4031 and to E-4031 in combination with AZD7009. In Purkinje fibres, but not in ventricular tissue, AZD7009 attenuated the E-4031-induced APD prolongation. In contrast, in atrial cells, AZD7009 further prolonged the APD. In addition, AZD7009 was able to suppress early afterdepolarisations (EADs) induced by E-4031 in Purkinje fibre preparations.

In conclusion, AZD7009 delays repolarisation and increases refractoriness in atrial tissue through synergistic inhibition of IK_r, I_{to}, IK_{ur} and INa, a mixed ion channel blockade that may underlie its high antiarrhythmic efficacy. Inhibition of the late sodium current, counteracting excessive APD prolongation and EADs in susceptible cells (midmyocardial and Purkinje cells), may explain the low proarrhythmic potential of AZD7009.

Key words: atrial fibrillation, antiarrhythmic drug, IK_r, IK_{ur}, I_{to}, IK_s, IK_{ACh}, INa, ICa_L, cardiac action potential, early afterdepolarisation

LIST OF PAPERS

This thesis is based on the following papers:

I. Persson F., Carlsson L., Duker G., Jacobson I. Blocking characteristics of hERG, hNav1.5 and hKvLQT1/hminK after administration of the novel antiarrhythmic compound AZD7009.
J Cardiovasc Electrophysiol 2005;16:329-341.

II. Persson F., Carlsson L., Duker G., Jacobson I. Blocking characteristics of hKv1.5 and hKv4.3/hKChIP2.2 after administration of the novel antiarrhythmic compound AZD7009.
J Cardiovasc Pharmacol 2005;46:7-17.

III. Persson F., Andersson B., Duker G., Jacobson I., Carlsson L. Functional effects of the late sodium current inhibition by AZD7009 and lidocaine in rabbit isolated atrial and ventricular tissue and Purkinje fibre.
Eur J Pharmacol, in press

IV. Persson F., Duker G., Hermansson N-O., Jacobson I., Carlsson L. Effects of AZD7009 on Kir3.1/Kir3.4 inward rectifier potassium current expressed in CHO cells.
Manuscript.

V. Persson F., Duker, G., Jacobson I., Carlsson L. Effects of AZD7009 on L-type calcium current in acutely isolated rabbit cardiomyocytes and H9c2 cells.
Manuscript.

CONTENTS

ABBREVIATIONS 7
INTRODUCTION 8
Electrical activity in the heart 8
Cardiac action potential 8
Phases of the cardiac action potential 8
Regional differences in APD 9
Correlation between the cardiac action potential and the ECG 10
Cardiac ion currents and ion channels 11
Sodium current (INa, Nav1.5) 12
L-type calcium current (ICa_L, Cav1.2) 13
T-type calcium current (ICa_T, Cav3.2) 13
Transient outward potassium current (I_{to}, Kv4.3) 13
Ultrarapid delayed rectifier potassium current (IK_{ur}, Kv1.5) 14
Rapid delayed rectifier potassium current (IK_r, hERG) 14
Slow delayed rectifier potassium current (IK_s, KvLQT1/minK) 15
Hyperpolarisation-activated nonselective cation current (I_f, HCN4) 15
Inward rectifier potassium current (IK_1, Kir2.1) 16
Acetylcholine-activated potassium current (IK_{ACh}, Kir3.1/Kir3.4) ... 16
ATP-sensitive potassium current (IK_{ATP}, Kir6.2/SUR2A) 16
Sodium calcium exchanger (I_{NCX}, NCX1) 17
Ion channel structure and function 17
Species differences 19
Atrial fibrillation 20
Mechanisms of atrial fibrillation 21
Remodeling 21
Antiarrhythmic drugs 22
Vaughan-Williams classification 22
Current pharmacological treatment of atrial fibrillation 23
Rate versus rhythm control 23
Proarrhythmia 24
Mechanisms of class III induced proarrhythmia 24
AZD7009 26
Electrophysiological characteristics 26
Efficacy 28
Low proarrhythmic potential 28
AIMS 29
MATERIALS AND METHODS 30
Animals (papers III, V) 30
Voltage-clamp experiments (papers I-V) 30
CHO cells, transfection and cell culturing (papers I-IV) 30

Isolation of cardiomyocytes (papers III, V) 31
H9c2 cells, cell culturing (paper V) 33
Voltage-clamp recordings (papers I-V) 33
Cell superfusion system (papers I-V) 36
Pulse protocols (papers I-V) 37
Activation, inactivation and deactivation (papers I, II, III, V) 38
Current-voltage curves (papers I, II, V) 39
Steady-state inactivation curves (papers I, II) 40
Concentration dependence of block (papers I-V) 41
Time course of block (papers I, II) 42
Use- and frequency-dependence of drug block (papers I, II, III) 43
Recovery from inactivation and use-dependent block (paper I) 44
Prepulse potentiation (paper I) 44
Fractional electric distance (paper II) 45
Currents in isolated cardiomyocytes (papers III, V) 45
Transmembrane action potential recordings (paper III) 46
Statistical analysis 48
RESULTS 49
Effects of AZD7009 on ion channels expressed in CHO cells 49
hERG current (paper I) 49
Nav1.5 current (papers I, III) 50
Kv4.3/KChIP2.2 current (paper II) 52
Kv1.5 current (paper II) 53
Kir3.1/Kir3.4 current (paper IV) 54
KvLQT1/minK current (paper I) 54
Summary of effects of AZD7009 on ion channels in CHO cells 55
Currents in isolated cardiomyocytes 57
Late sodium current (paper III) 57
L-type calcium current (paper V) 58
L-type calcium current in H9c2 cells (paper V) 58
Transmembrane action potentials (paper III) 59
GENERAL DISCUSSION 61
Characteristics of ion channel blockade by AZD7009 61
Mechanisms underlying the predominant atrial effects of AZD7009 64
Mechanisms underlying the high antiarrhythmic efficacy of AZD7009 65
Mechanisms underlying the low proarrhythmic potential of AZD7009 66
CONCLUSIONS 69
FUTURE DIRECTIONS 70
POPULÄRVETENSKAPLIG SAMMANFATTNING 71
ACKNOWELEDGEMENTS 74
REFERENCES 75

ABBREVIATIONS

ACh	acetylcholine
AF	atrial fibrillation
AERP	atrial effective refractory period
APD	action potential duration
ATP	adenosine triphosphate
AUC	area under the curve
AV node	atrioventricular node
EAD	early afterdepolarisation
ECG	electrocardiogram
ERP	effective refractory period
hERG	human ether-a-go-go related gene
HEPES	N-(hydroxyethyl)piperazine-N'-(2-ethanesulfonic acid)
I	current
ICa	calcium current
ICa_L	L-type calcium current
ICa_T	T-type calcium current
IK_{Ach}	acetylcholine sensitive potassium current
IK_1	inward rectifier potassium current
IK_r	rapid delayed rectifier potassium current
IK_s	slow delayed rectifier potassium current
IK_{ur}	ultra rapid delayed rectifier potassium current
INa	sodium current
INa_{late}	late sodium current
INa_{peak}	peak sodium current
I_{to}	transient outward potassium current
K_{ir}	inward rectifier potassium channel
K_v	voltage-gated potassium channel
M cell	midmyocardial cell
SA node	sinoatrial node
TdP	Torsades de Pointes
VERP	ventricular effective refractory period

INTRODUCTION

Electrical activity in the heart

The heart beat is triggered by a wave of electrical activity starting in the sinoatrial node (SA node) located in the right atrium. The electrical impulse travels through the atria to the atrioventricular node (AV node) and passes down the His bundle branches and Purkinje fibres into the ventricular myocardium. The electrical impulse induces an increase in the concentration of intracellular Ca^{2+} which in turn leads to contraction of the heart.

Cardiac action potential

The resting membrane potential in atrial, ventricular and Purkinje cells is about -80 mV whereas the resting membrane potential in the pacemaker cells is less negative, -50 to -60 mV in the SA node and -60 to -70 mV in the AV node. The cardiac action potential is generated by sequential activation and inactivation of ion channels and ion pumps that conduct inward, depolarising (Na^+ and Ca^{2+}) currents and outward, repolarising (K^+) currents (Nerbonne et al., 2005). Ion channels and ion pumps are proteins that traverse the cell membrane and are able to pass ions from inside to outside the cell or vice versa. The flow of ions through ion channels is passive and determined by the ion concentration and the electrical gradient over the cell membrane, whereas the transport of ions via ion pumps is an active and energy consuming process and may move ions against concentration and electrical gradients. Depending on cell type and localisation in the heart, the duration of the normal human cardiac action potential in atrial cells is 200 to 300 ms and in ventricular cells 250 to 450 ms (Boutjdir et al., 1986; Li et al., 1998). Following the initiation of an action potential, a certain time period, the refractory period, must pass before a new action potential can be elicited. This is due to the inability of depolarising ion channels to activate unless they have first returned to a rested closed state. Consequently, the heart alternates between contraction and rest, i.e. systole and diastole, respectively.

Phases of the cardiac action potential

By convention, the cardiac action potential is divided into five phases: phase 0 through phase 4 (Figure 1). Phase 0 is the initiation and rapid depolarisation of the action potential from the negative resting potential to positive potentials (+30 to +40 mV). Phase 1 is the early and partial

repolarisation that brings down the potential towards a plateau. Phase 2 is the plateau during which the potential remains near 0 mV and phase 3 is the final repolarisation that brings the potential down towards the negative resting potential. Finally, phase 4 is the time spent at the resting membrane potential until a new action potential is elicited.

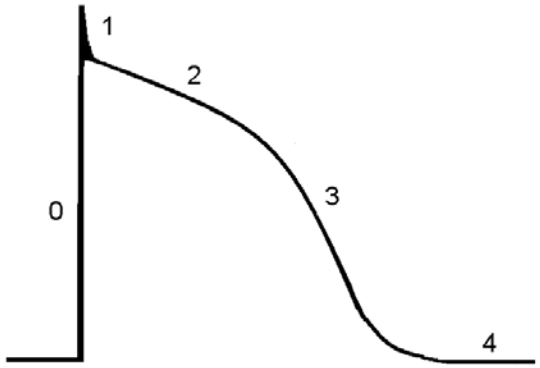

Figure 1. The phases of the cardiac action potential, phase 0 – depolarisation, phase 1 – early repolarisation, phase 2 – plateau, phase 3 – final repolarisation and phase 4 – diastole

Regional differences in APD

Due to differences in the expression and function of ion channels and ion pumps, the cardiomyocyte action potential has different configurations and durations in different regions of the heart (Figure 2). The cells in the atrium, His bundle, Purkinje fibre and ventricle have fast depolarisation carried by the cardiac Na^+ current, whereas the cells in the SA node and AV node have slow depolarisation carried by the L-type Ca^{2+} current. The cells in the SA node and the AV node display automaticity, i.e. they are able to fire action potentials without a previous stimuli, owing to a slow depolarisation induced by the unspecific cation current I_f and the T-type Ca^{2+} current. Automaticity is also seen in the cells of the His/Purkinje system, although at a much slower frequency.

The duration and configuration of the action potential repolarisation differ considerably between different types of cardiac cells (Figure 2). In the atrium, the action potential is short with an evenly distributed repolarisation and a brief plateau (Courtemanche et al., 1999). The action potential in the His/Purkinje system is long, typically with a notch before a pronounced plateau, giving rise to a spike and dome appearance. In the ventricle, the action potential differs considerably depending on the transmural location of the cell; the epicardial cells have the shortest action potentials, the midmyocardial cells (M cells) have the longest action potentials, and the duration of the endocardial action potentials is between these (Drouin et al., 1995; Li et al., 1998). Epicardial cells have action potentials with a clearly visible notch before the plateau while endocardial cells do not. The action

potential in Purkinje fibre cells is in many ways similar to the action potential in M cells, such as the long duration of the plateau and the pronounced spike and dome appearance.

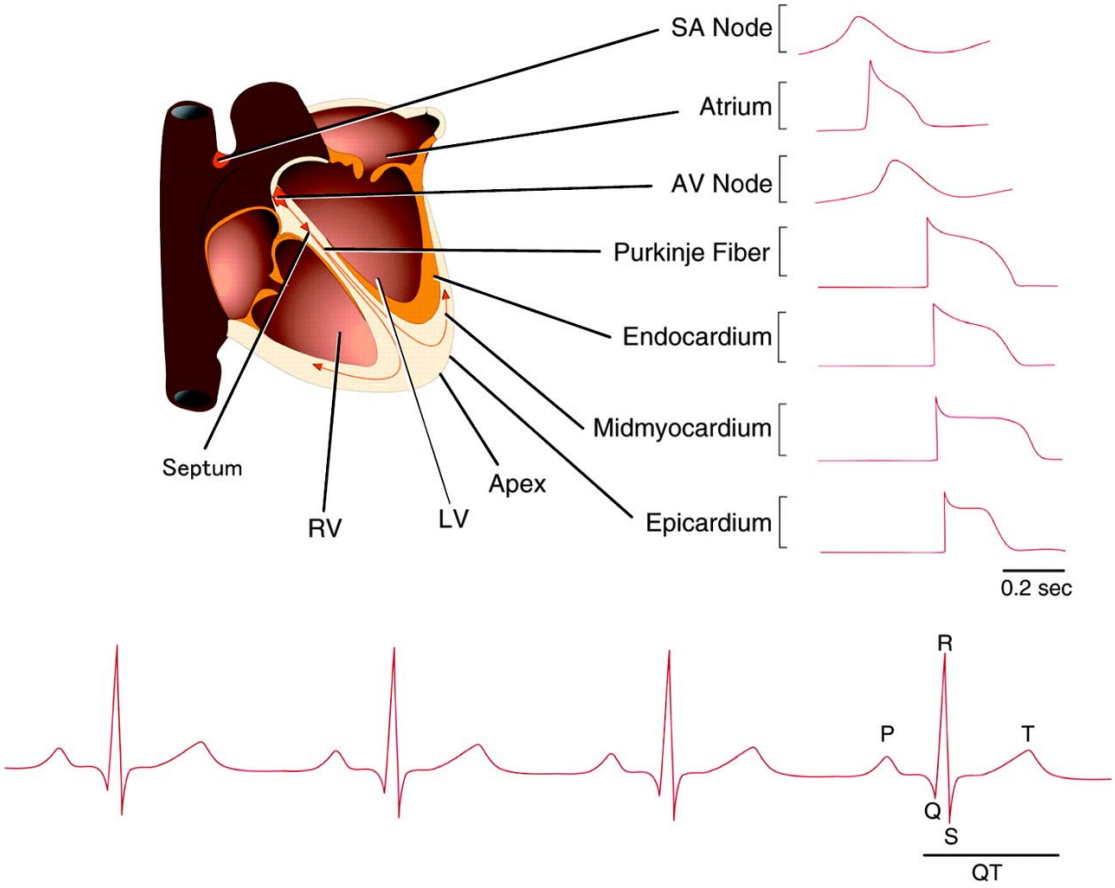

Figure 2. Action potentials from different regions of the heart and their correlation to the ECG, see text below. From Nerbonne and Kass, 2005, Physiol Rev 85:1205-1253, used with permission.

Correlation between the cardiac action potential and the ECG

Figure 2 shows the relation between the cardiac action potentials in different regions of the heart and the surface electrocardiogram (ECG). The P wave corresponds to the depolarisation of the atria. The isoelectric segment between the end of the P wave and the start of the QRS complex mainly reflects the propagation of the electrical impulse through the AV node. The QRS complex corresponds to depolarisation of the ventricles spreading to the ventricular apex and the endocardium and further towards the base and the epicardium. The ST segment corresponds to the plateau of the ventricular action potential, where all ventricular cells are depolarised. The T wave represents the ventricular repolarisation starting with epicardial cells and ending with M cells (Yan et al., 1998). The duration from the peak to the end of the T wave has been suggested to represent the transmural

dispersion of repolarisation in the ventricle, and the interval between the start of the QRS complex and the end of the T wave, the QT interval, represents the time from initial depolarisation to final repolarisation of the ventricle. Since the duration of the ventricular action potential is shortened at higher stimulation frequencies, a pronounced frequency dependence is also seen for the QT interval, with shorter a QT interval at higher frequency (Carmeliet et al., 2002a).

Cardiac ion currents and ion channels

Schematic drawings of the major ion currents active during the different phases of the action potential in ventricular and atrial myocytes are shown in Figure 3.

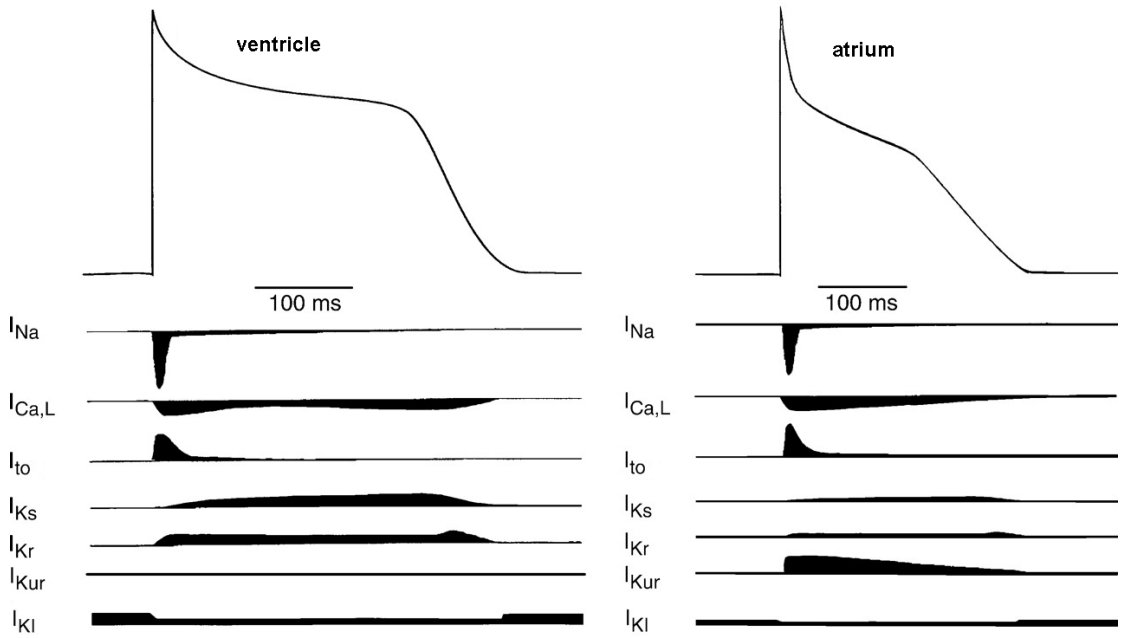

Figure 3. Action potential configuration and underlying currents in human ventricular and atrial myocytes. Downward projections indicate inward depolarising currents and upward projections indicate outward repolarising currents. Modified from Nerbonne and Kass, 2005, Physiol Rev 85:1205-1253, used with permission.

See Nerbonne et al. for an extensive review of the cardiac ion currents and their ion channel correlates (Nerbonne et al., 2005). The following describes the major cardiac ion currents, ion channels and their function during the cardiac action potential in more detail. The major cardiac ion currents and the corresponding ion channels and genes are summarized in Table 1. In addition to these ion currents, several other ion currents are present in cardiac tissue, such as Cl^- currents, background K^+ currents (TWIK-1, TASK etc.), stretch-activated currents and current generating ion

pumps, e.g. Na^+/K^+ ATPase. However, a description of these currents is beyond the scope of this thesis. See Carmeliet et al. for a review of these currents (Carmeliet et al., 2002b).

Table 1 Major cardiac ion currents and corresponding ion channels and genes

Ion current	Ion channel	Gene
INa	Nav1.5	SCN5A
ICa_L	Cav1.2	CACNA1C
ICa_T	Cav3.2	CACNA1H
I_{to}	Kv4.3	KCND3
	KChIP2	KCNIP2
IK_{ur}	Kv1.5	KCNA5
IK_r	hERG	hERG/KCNH2
IK_s	KvLQT1	KCNQ1
	minK	KCNE1
I_f	HCN4	HCN4
IK_1	Kir2.1	KCNJ2
IK_{ACh}	Kir3.1	KCNJ3
	Kir3.4	KCNJ5
IK_{ATP}	Kir6.2	KCNJ11
	SUR2A	ABCC9
I_{NCX}	NCX1	NCX1

Sodium current (INa, Nav1.5)

The cardiac sodium current (INa) has fast activation and inactivation kinetics and is responsible for the rapid upstroke of the action potential (phase 0) in atrial, ventricular, Purkinje and His bundle cells. The cardiac sodium current runs through the sodium channel Nav1.5 (formerly known as hH1) encoded by the gene SCN5A (Gellens et al., 1992). A small sustained component of the sodium current, the late sodium current (INa_{late}), is also active during phase 2 and phase 3 and contributes to determining the APD (Maltsev et al., 1998). INa_{late} in human cardiomyocytes is thought to comprise two gating modes, burst openings and late scattered openings (Maltsev et al., 2006; Undrovinas et al., 2002). The late sodium current is an important contributor to the generation of early afterdepolarisations (EADs) (Fedida et al., 2006). EADs are secondary depolarisations occurring during the action potential repolarisation and are discussed in greater detail in the section on proarrhythmia below.

L-type calcium current (ICa_L, Cav1.2)

The L-type Ca^{2+} channel belongs to the group of high voltage activated calcium channels (Striessnig, 1999). The α-subunit of the cardiac L-type Ca^{2+} channel is Cav1.2, which is encoded by the CACNA1C gene. Accessory subunits are needed to form functional channels, e.g. the cytosolic β-subunit and the membrane bound α2-δ-subunit. The L-type calcium current (ICa_L) is present in all cardiac cells and is important for the excitation-contraction coupling. In atrial and ventricular cells, ICa_L is active during the action potential plateau. In pacemaker cells (SA node and AV node), ICa_L contributes to the slow action potential depolarisation (Mangoni et al., 2006). At high rates, APD shortens as a consequence of an incomplete recovery from inactivation of ICa_L and faster inactivation upon an elevated intracellular Ca^{2+} concentration.

T-type calcium current (ICa_T, Cav3.2)

The α-subunit of the T-type calcium channel Cav3.2 is encoded by the CACNA1H gene (Cribbs et al., 1998). The T-type Ca^{2+} current (ICa_T) activates at lower potential, i.e. is low voltage activated, and inactivates more rapidly than ICa_L, resulting in a transient current. T-type calcium current is present in pacemaker cells and the conduction system of the heart (SA node, AV node and Purkinje fibre) (Mangoni et al., 2006). In most mammalian species ICa_T is also present in the atrium and ventricle, and mRNA for Cav3.2 has been found in human atrium and ventricle. However, it has not yet been possible to detect the current in isolated human cardiomyocytes (Gaborit et al., 2005; Vassort et al., 2006).

Transient outward potassium current (I_{to}, Kv4.3)

The transient outward potassium current (I_{to}, also called I_{to1} and I_{tof}) has fast activation and inactivation kinetics and contributes to the early repolarisation (phase 1) of the action potential in atrial and ventricular myocytes (Oudit et al., 2001). The channel protein underlying I_{to} differs among different mammalian species (see the discussion on species differencies below). In humans, the α-subunit Kv4.3 underlies I_{to} and is encoded by the KCND3 gene (Dixon et al., 1996; Kong et al., 1998). Expression of Kv4.3 alone gives a current that resembles I_{to} in human cardiomyocytes, but coexpression with the accessory protein KChIP2 makes the current even more similar to native I_{to} (Decher et al., 2001). KChIP2 is encoded by the KCNIP2 gene and, when coexpressed with Kv4.3, the inactivation becomes slower and the recovery from inactivation faster. In addition, when coexpressed with KChIP2, the current amplitude

of Kv4.3 is much larger (up to 100-fold) than the current amplitude of Kv4.3 alone, as a result of KChIP2 increasing the cell surface expression of Kv4.3 (An et al., 2000; Bähring et al., 2001). The distribution of KChIP2 in the ventricle is parallel to the I_{to} gradient, with a large I_{to} in the epicardium and a small I_{to} in the endocardium, but the role of KChIP2 in shaping the I_{to} gradient is not fully understood (Pourrier et al., 2003; Rosati et al., 2001).

Ultrarapid delayed rectifier potassium current (IK_{ur}, Kv1.5)

The α-subunit Kv1.5, encoded by the KCNA5 gene, underlies the ultra rapid delayed rectifier potassium current (IK_{ur}, also called I_{so} or I_{sus}) (Tamkun et al., 1991; Wang et al., 1993). IK_{ur} is found in human atrium but not in the ventricle or Purkinje fiber (Amos et al., 1996). IK_{ur} activates rapidly (much faster as compared to IK_r, see below) and remains active during the action potential plateau (phase 2) and the final repolarisation (phase 3). Wettwer et al. recently reported that inhibition of IK_{ur} in atrial myocytes isolated from patients with AF resulted in prolongation of the APD at final repolarisation, whereas inhibition of IK_{ur} in atrial myocytes from patients in sinus rhythm resulted in a shortening of the APD (Wettwer et al., 2004). The discrepancy may be explained by differences in the amount of ICa_L (see electrical remodeling below). When IK_{ur} is inhibited in normal cardiomyocytes, the resulting delay in early repolarisation and elevation of the action potential plateau leads to a prolonged activation of ICa_L followed by an increased activation of the late repolarising currents, IK_r and IK_s, and consequently an accelerated late repolarisation. The accelerated late repolarisation may neutralize the delay of the early repolarisation and the plateau, resulting in no net APD prolongation or even an APD shortening. Since the amount of ICa_L is profoundly decreased in remodelled cardiomyocytes (Bosch et al., 1999; Brundel et al., 1999), inhibition of IK_{ur} prolongs the APD as a direct result of the decreased repolarising current, and the resulting prolonged activation of ICa_L is too small to have any impact on the activation of the late repolarising currents.

Rapid delayed rectifier potassium current (IK_r, hERG)

The α-subunit responsible for the rapid delayed rectifier potassium current (IK_r) is encoded by the human-ether-a-go-go related gene (hERG also called KCNH2) (Sanguinetti et al., 1995; Trudeau et al., 1995). hERG was first cloned from human hippocampus but it is also highly expressed in the heart (Warmke et al., 1994). The role of accessory subunits for formation of IK_r *in vivo* is unclear; an association with minK and MiRP1 has been proposed but no consensus has been reached as yet (Anantharam et al., 2005). IK_r is important during the final repolarisation of the action potential

(phase 3). The hERG channel has very characteristic biophysical properties that distinguish it from the other Kv channels (Tseng, 2001; Vandenberg et al., 2004). At the resting membrane potential, the hERG channel is closed and channel activation has a threshold at -40 to -30 mV. When the activation threshold is reached the hERG channel activates but inactivates rapidly at depolarised potentials. As a result, the outward current peaks at already 0 to +10 mV, although maximal activation is not reached until the membrane potential is +20 to +30 mV. Upon return to repolarised potentials, the recovery from inactivation is faster than the deactivation of the channel, resulting in a large repolarising current during the final repolarisation.

Slow delayed rectifier potassium current (IK_s, KvLQT1/minK)

Coexpression of the α-subunit KvLQT1 encoded by the KCNQ1 gene and the β-subunit minK (also called IsK) encoded by the KCNE1 gene results in a current similar to the slow delayed rectifier potassium current (IK_s) seen in cardiaomyocytes (Barhanin et al., 1996; Sanguinetti et al., 1996). The role of IK_s during the cardiac action potential repolarisation has not been fully elucidated. It has been suggested that the impact of IK_s increases during β-adrenergic receptor stimulation during which IK_s activates faster. The impact of IK_s is also increased during inhibition of IK_r when IK_s limits repolarisation instability at higher heart rates due to incomplete deactivation between action potentials (Jost et al., 2005; van Ginneken et al., 1999; Volders et al., 2003).

Hyperpolarisation-activated nonselective cation current (I_f, HCN4)

The hyperpolarisation-activated nonselective cation current (also called pacemaker current or funny current, I_f) is an inwardly directed current active during phase 4 of the cardiac action potential. I_f initiates the slow diastolic depolarisation that generates the spontaneous, repetitive activity in the pacemaking cells of the heart (DiFrancesco, 2006). The channel responsible for I_f is the hyperpolarisation-activated, cyclic nucleotide-gated cation channel (HCN). In the heart, HCN4 is the main subtype, although expression of HCN1 and HCN2 has been reported as well (Baruscotti et al., 2005). The structure of the HCN channel is similar to that of Kv channels; in addition the HCN channels have a cyclic nucleotide-binding domain in the C-terminus. The current is carried by Na^+ and K^+ ions and activates slowly at membrane potentials negative to -40 mV.
I_f does not influence the electrophysiological properties of adult atrial and ventricular cells under normal physiological conditions but in certain pathophysiological conditions such as heart failure and hypertrophy an

upregulation of I_f linking those conditions to atrial and ventricular arrhythmias may occur (Cerbai et al., 2006).

Inward rectifier potassium current (IK_1, Kir2.1)

The molecular correlate to the inward rectifier potassium current (IK_1) in the heart is thought to be Kir2.1, which is encoded by the KCNJ2 gene (Kubo et al., 1993). In addition to Kir2.1, Kir2.2 may coassemble with Kir2.1 into heteromultimeric channels (Zobel et al., 2003). IK_1 is present in both atrial and ventricular myocytes and contributes to maintaining the resting membrane potential and shaping the initial depolarisation and the final repolarisation of the cardiac action potential (Lopatin et al., 2001). IK_1 is about six times larger in ventricular cells than in atrial cells.

Acetylcholine-activated potassium current (IK_{ACh}, Kir3.1/Kir3.4)

The acetylcholine-activated K^+ channel is composed of two different subunits, Kir3.1 and Kir3.4. Kir3.1 (also called GIRK1) is encoded by the KCNJ3 gene and Kir3.4 (also called GIRK4) by KCNJ5. The functional acetylcholine-activated K^+ current (IK_{ACh}) channel is formed by coassembly of two Kir3.1 subunits and two Kir3.4 subunits (Krapivinsky et al., 1995). IK_{ACh} is present in atrial myocytes where it contributes (together with IK_1) to determining the resting membrane potential, the action potential duration and the refractory period. IK_{ACh} is also present in myocytes from the conduction system (SA node, AV node and Purkinje fibre) where it mediates a vagally induced slowing of the heart rate (Yamada, 2002; Yamada et al., 1998). IK_{ACh} is not expressed in ventricular myocytes. IK_{ACh} is G-protein coupled and activates upon vagal stimulation when ACh binds to and activates the M2 muscarinic receptor. The M2 muscarinic receptor is coupled to the pertussis toxin-sensitive G protein complex (Gi). Upon activation the complex dissociates into Gα and Gβγ (Wickman et al., 1999). The Gβγ subunit directly activates the IK_{ACh} potassium channel (Sadja et al., 2003).

ATP-sensitive potassium current (IK_{ATP}, Kir6.2/SUR2A)

The ATP-sensitive potassium channel is formed by coassembly of four inward rectifier potassium channel subunits (Kir6.2 encoded by the KCNJ11 gene) and four sulfonylurea receptors (SUR2A encoded by the ABCC9 gene) (Lorenz et al., 1999). SUR2A belongs to the ATP binding cassette proteins and renders the channel-complex sensitive to ATP. IK_{ATP} is found in all cell types in the human heart and activates when the intracellular concentration of ATP is decreased, for example during ischemia, resulting in a decreased APD and thereby a decreased influx of

Ca^{2+} (Kane et al., 2005). Hence, IK_{ATP} has a cardioprotective role during myocardial stress.

Sodium calcium exchanger (I_{NCX}, NCX1)

During diastole (phase 4) the sodium calcium exchanger extrudes Ca^{2+} from the cardiomyocyte (forward mode). One Ca^{2+} ion is exchanged for three Na^{+} ions, leading to an inwardly directed current, thus contributing to depolarisation. In conditions such as heart failure and ischemia that cause Ca^{2+} overload, the sodium calcium exchanger may elicit delayed afterdepolarisations (Noble et al., 2006; Shiroshita-Takeshita et al., 2005). At depolarised potentials (above –50 mV), the exchanger runs in the reverse mode, moving calcium into and sodium out of the cell and causing an outwardly directed repolarising current. However, when the intracellular Ca^{2+} concentration is increased, the reversal potential of the sodium calcium exchanger is moved towards potentials that are more positive than the action potential plateau and hence the current becomes inwardly directed again (Bett et al., 1992). The cardiac sodium calcium exchanger is encoded by the NCX1 gene (Shieh et al., 1992).

Ion channel structure and function

The α-subunits of voltage-gated ion channels are built up of four domains (Na^{+} and Ca^{2+} channels) or subunits (K^{+} channels), each containing six transmembrane spanning (6TM) α-helices (S1 to S6), one pore loop and intracellular N- and C-terminal domains (Figure 4) (Roden et al., 2002). The first crystal structure of an ion channel was provided in 1998 for the bacterial potassium channel KcsA. The KcsA structure shows a transmembrane tetramer with an aqueous pore in the middle and a selectivity filter at the narrowest part of the pore. A large aqueous cavity (the inner vestibule) is located at the cytoplasmic side of the selectivity filter and narrows near the cytoplasmic part of the channel (the gate) (Doyle et al., 1998). A mammalian potassium channel belonging to the Kv channel family has later been shown to have a structure similar to that of KcsA (Long et al., 2005). The ion permeability of different ion channels is determined by the aminoacid sequence in the selectivity filter, e.g. the Gly-X-Gly aminoacid sequence represents a K^{+} channel. Voltage gating is regulated by the fourth transmembrane α-helix, which contains many positively charged arginine residues (Figure 4). When the membrane is depolarised, the fourth transmembrane α-helix moves in the electric field and induces conformational changes in the ion channel protein that open the

gate and transform the ion channel from a closed into an open or activated ion conducting state (Jiang et al., 2003).

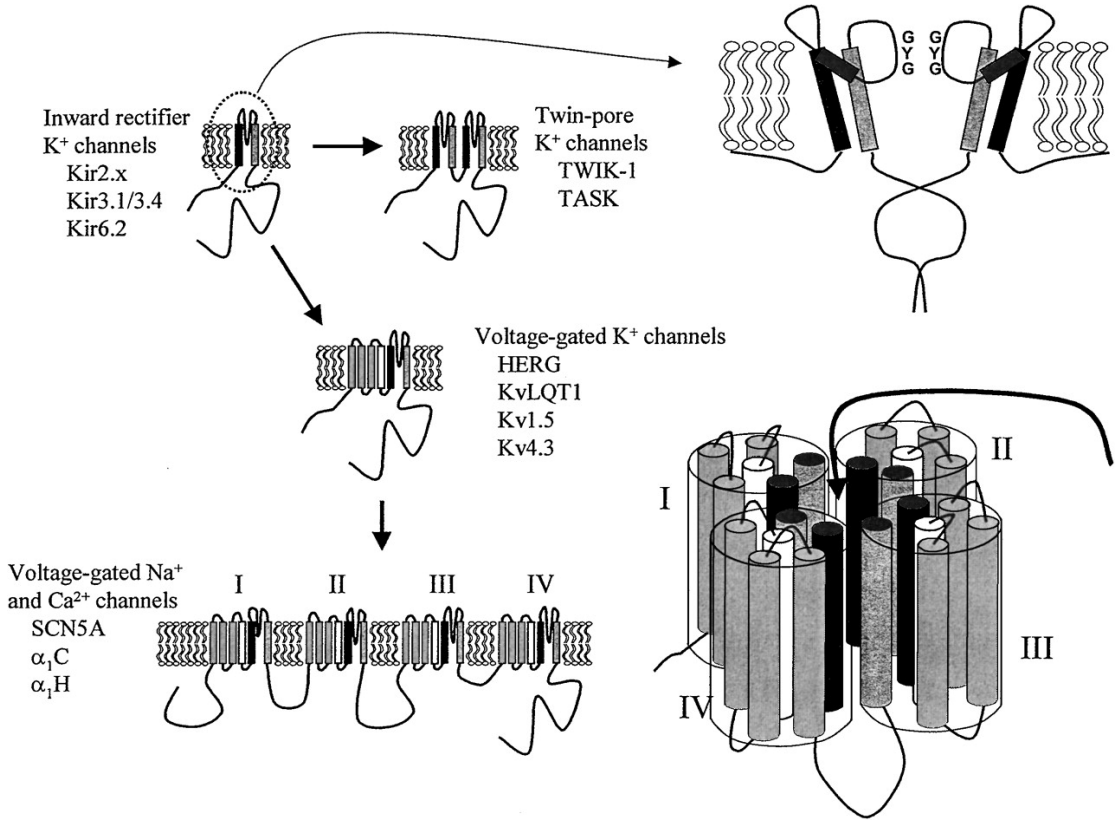

Figure 4. An evolutionary view of the structure of ion channels. The inward rectifier K^+ channels have the simplest structure with only two transmembrane spanning α-helices and one pore loop. The voltage-gated K^+ channels consist of six transmembrane spanning α-helices and one pore loop. Four subunits of the inward rectifier or the voltage-gated K^+ channels coassemble to form one ion channel. In the voltage-gated Na^+ and Ca^{2+} channels, four domains are present within the same protein. The twin-pore K^+ channels (background channels) are not further discussed. Reprinted with permission by the Annual Review of Physiology, Volume 64 © 2002, by Annual Reviews www.annualreviews.org, Roden, 2002, 64:431-475.

Most voltage-gated ion channels are transformed into a non-conducting state by an inactivation process that occurs during prolonged depolarisation, e.g. during the cardiac action potential plateau. The amount and velocity of the inactivation vary considerably between different ion channels. Two major inactivation mechanisms have been described: N-type inactivation, which involves occlusion of the channel through the binding of a short segment of amino acid residues at the N-terminal, and C-type inactivation, which involves conformational changes of amino acid residues near the pore (Rasmusson et al., 1998). Upon return towards more repolarised potentials, and finally the resting membrane potential, the voltage-gated ion channels close.

Similar to the α-subunits of the voltage-gated ion channels, the inward rectifier potassium channels (responsible for IK_1, IK_{ACh} and IK_{ATP}) consist of four subunits, but each subunit has only two transmembrane-spanning α-helices (2TM) and one pore loop (Figure 4) (Dhamoon et al., 2005). Inward rectification is achieved by the voltage-dependent channel inhibition by Mg^{2+} ions and positively charged intracellular polyamines, such as spermine, that plug the pore at depolarised membrane potentials (Makary et al., 2005).

Several accessory subunits coassemble with the α-subunits in order to regulate the function of the ion channels (Li et al., 2006). Four different Kvβ subunits have been identified so far (Kvβ1 to Kvβ4); in addition, several variants may exist, e.g. Kvβ1.1 and Kvβ1.2. The Kvβ subunits have been shown to influence the kinetics of activation and inactivation of several ion channels. Four β-subunits that modulate the sodium channel have been identified in cardiomyocytes (Navβ1 through Navβ4 encoded by SCN1B through SCN4B) (Herfst et al., 2004). The exact functional role of the sodium channel β-subunits is not fully known, but they are thought to modulate channel gating and cell surface expression and to interact with cell adhesion molecules. Another type of accessory subunit is the K^+ channel interacting protein (KChIP) (An et al., 2000). The KChIPs interact with Kv4 subunits; see the above section on I_{to}. The KCNE genes (KCNE1-KCNE5) encode proteins with an extracellular N-terminal, a single transmembrane domain and a cytoplasmic C-terminal. In the heart, KCNE1 encodes minK, which coassembles with KvLQT1 to form IK_s; two minK subunits are thought to coassemble with one KvLQT1 subunit (Barhanin et al., 1996; Sanguinetti et al., 1996). MinK has also been proposed to coassemble with hERG (Yang et al., 1995). KCNE2 encodes MiRP1, which is thought to coassemble with hERG (Abbott et al., 1999; Mazhari et al., 2001), KvLQT1 (Tinel et al., 2000), Kv4 (Zhang et al., 2001) and HCN (Yu et al., 2001).

Species differences

The expression of cardiac ion channels varies between different mammalian species, a fact that must be taken into consideration in using animal tissue for ion channel research (Nerbonne, 2000; Nerbonne et al., 2005). The most obvious example is the variation of the molecular correlate of I_{to}. I_{to} inactivates rapidly in human and dog cardiomyocytes, whereas I_{to} in rabbit cardiomyocytes has considerably slower inactivation kinetics. In the dog and man, Kv4.3 is responsible for I_{to} while Kv1.4 in combination with

Kv4.2 and Kv4.3 are responsible for I_{to} in the rabbit (Dixon et al., 1996; Wang et al., 1999).

The molecular correlate of IK_{ur} is Kv1.5. In humans IK_{ur} is found in the atria but not in the ventricles (Amos et al., 1996; Feng et al., 1997). Although IK_{ur} was not found in human ventricular myocytes, Kv1.5 mRNA has been reported to be present in human ventricle (Ördög et al., 2006). In dogs Kv1.5 is now thought to be the molecular correlate to IK_{ur} (Fedida et al., 2003) although Kv3.1 has also been suggested (Yue et al., 2000). While the Kv1.5 protein has been found in dog atria and ventricle, the electrophysiological correlate to Kv1.5 in the ventricle remaines to be clarified (Fedida et al., 2003). The presence and location of IK_{ur} in rabbits are less clear, Kv1.5 mRNA has been found in both atria and ventricle (Sasaki et al., 1995) but the presence of the Kv1.5 protein or IK_{ur} has not been studied in the rabbit. In goats, Kv1.5 mRNA is found in the atria (van der Velden et al., 2000).

IK_r is present in different regions (atrium and ventricle) in rabbit, dog and human hearts (Wymore et al., 1997). Similar to IK_r, IK_s is present in rabbit, dog and human hearts (Li et al., 1996; Liu et al., 1995; Salata et al., 1996).

Atrial fibrillation

Atrial fibrillation is characterized by an uncoordinated, rapid activity (>400 beats/min) in the atria leading to deterioration of the atrial mechanical function. It is associated with several complications, e.g. thromboembolic events due to the impaired atrial contraction that predisposes to the formation of atrial thrombosis and impairment of ventricular function. In addition, AF is associated with decreased long-term survival. Patients suffering from AF display symptoms such as palpitations, dizziness, fatigue, breathlessness and chest pain (Authors/Task Force Members et al., 2006).

Atrial fibrillation is the most common arrhythmia in clinical practice; approximately 4.5 million people in the European Union have paroxysmal or persistent AF. The prevalence of AF is 0.4 to 1% in the general population but increases with age up to 8% in persons older than 80 years. As the percentage of elderly individuals within the population increases, AF is emerging as an important public health concern.

Atrial fibrillation is classified according to the duration and recurrence of the fibrillation episodes. The condition is called recurrent AF when a patient has had two or more episodes, paroxysmal AF when the fibrillation spontaneously terminates, persistent AF when the fibrillation episode is sustained beyond seven days and intervention is needed for its termination, and permanent AF is long-standing AF where attempts to restore sinus rhythm have failed. The disease normally progresses from paroxysmal to persistent and finally to permanent AF.

Mechanisms of atrial fibrillation

The mechanisms behind AF are not fully known but theories concerning ectopic foci and multicircuit reentry are most commonly described, for a review see (Nattel et al., 2000). Single or multiple ectopic foci are often located in the orifice of the pulmonary veins; due to inhomogeneities in atrial conduction, the ectopic beats may travel through the atria in an irregular fashion, causing AF. Multicircuit reentry arises when the depolarisation wavefront bifurcates into multiple wavefronts due to dynamic or structural conduction inhomogeneities within the atria.

Since the circumference of the smallest reentry circuit that can exist is defined by the product of the ERP and the conduction velocity, shortening of the ERP and/or a reduction of the conduction velocity will facilitate multicircuit reentry. Due to structural and electrical remodeling (see below) that shorten the reentrant wavelength and cause conduction inhomogeneities in the atria, the maintenance of AF is thought to be governed by multicircuit reentry, irrespective of the original cause of the disease.

Remodeling

AF will result in progressively decreased atrial APD and ERP, increased heterogeneity of atrial APD and ERP and altered APD/ERP frequency relationships (Boutjdir et al., 1986; Wijffels et al., 1995). In addition, the atrial conduction velocity is decreased in an inhomogenous fashion. These changes may be explained by the electrical and structural remodeling induced by AF. The first demonstration of high frequency pacing inducing changes in atrial electrophysiology and promoting the occurrence and maintenance of AF, i.e. that AF begets AF, was reported by Wijffels et al. (Wijffels et al., 1995). A clinical consequence of atrial remodeling is that the longer the time spent in AF, the more resistant the arrhythmia becomes to therapy.

Electrical remodeling includes changes in ion channel expression and function in atrial myocytes (Dobrev et al., 2003; Shiroshita-Takeshita et al., 2005). In atrial myocytes from AF patients, ICa_L is downregulated by approximately 70% and, in accordance, both the mRNA and the protein levels of the α-subunit Cav1.2 are reduced (Bosch et al., 1999; Brundel et al., 1999). This reduction in ICa_L contributes to the loss of the action potential plateau in atrial myocytes. Reductions of INa have been noted in dogs with tachycardia-induced AF (Gaspo et al., 1997), but to date there is no evidence of a decreased INa in atrial myocytes from AF patients, although a positive shift in the steady-state inactivation curve has been described (Bosch et al., 1999). The inward rectifier IK_1 is increased at the current, protein and mRNA levels in atrial myocytes from AF patients (Bosch et al., 1999). Increased basal inward rectifier K^+ current shortens the APD and, hence, increases atrial vulnerability to tachyarrhythmia and AF. It was recently noted that the increased basal inward rectifier K^+ current may be partly due to agonist-independent constitutively active IK_{ACh} (Dobrev et al., 2005). It should be noted however that both expression (protein and mRNA) of the ion channel subunits responsible for IK_{ACh}, Kir3.1 and Kir3.4 as well as the current in response to M2 muscarinic receptor stimulation are decreased in the fibrillating atria. Large reductions of I_{to} have been reported at current, protein and mRNA levels (Bosch et al., 1999; Brundel et al., 2001). There are conflicting results in the case of IK_{ur} with some studies showing a decrease and some no change in IK_{ur} in atrial myocytes from AF patients (Dobrev et al., 2003). It is complicated to predict the effects of decreased early repolarising currents on the APD since they influence the amount of activation of inward and outward currents during the later stages of the action potential; see the discussion on IK_{ur} on p14.

In structural remodeling, fibrosis develops between and within atrial muscle bundles leading to conduction disturbancies that may stabilise AF. Structural remodeling may be one of the connections between AF and heart failure (Li et al., 1999; Shiroshita-Takeshita et al., 2005).

Antiarrhythmic drugs

Vaughan-Williams classification

Antiarrhythmic drugs have traditionally been classified according to the Vaughan-Williams scheme (Vaughan-Williams, 1970). Class I drugs are drugs that inhibit the cardiac sodium channel and are further divided into

class IA, IB or IC depending on the kinetics of onset and recovery from the rate-dependent block of the cardiac sodium channel (Campbell, 1989). Class IA drugs (e.g. quinidine, procainamid and disopyramide) have an intermediate rate, class IB drugs (e.g. lidocaine and mexiletine) have a fast rate and class IC drugs (e.g. flecainide and propafenone) have a slow rate of onset and recovery from rate-dependent block. Class II drugs are drugs that inhibit the β-adrenoceptor (β-blockers, e.g. propranolol) and thereby attenuate the sympathetic influence on the heart. Class III drugs (e.g. dofetilide and ibutilide) delay action potential repolarisation by inhibiting repolarising potassium currents, preferentially IK_r. Class IV drugs (e.g. verapamil and diltiazem) inhibit the L-type Ca^{2+} channel. A problem with the Vaughan Williams classification system is that several antiarrhythmic drugs display properties of more than one class, for example sotalol and amiodarone, which are usually referred to as class III agents but also display features of class II (sotalol) and classes I, II and IV (amiodarone).

Current pharmacological treatment of atrial fibrillation

The multitude of antiarrhythmic drugs influencing atrial electrophysiology that can be used for management of AF primarily reflect the fact that no superior and safe treatment exists (Camm, 2006). Hence, there is still a great need to identify pharmacological options to manage AF in an effective and safe manner. Two different pharmacological treatment strategies for AF are currently used: rhythm control and rate control. The intention of the rhythm control strategy is to convert AF to and to maintain sinus rhythm. Class IA (e.g. quinidine), class IC (e.g. flecainide) and class III (e.g. ibutilide, amiodarone) antiarrhythmic drugs may be used for rhythm control. Unfortunately, these drugs all have the potential to induce ventricular proarrhythmia (see below). The rate control strategy, the intention of which is to control the ventricular rate during AF, includes class II (e.g propranolol) and class IV drugs (e.g. verapamil). In addition to the rhythm or rate-controlling drugs, anticoagulation therapy is needed to prevent thromboembolic events, e.g. stroke.

Rate versus rhythm control

With the unexpected outcome that rate control was not inferior to rhythm control, an intense discussion of the benefit / risk of either therapy started and is still ongoing (Crijns, 2005). A major problem in the studies made so far and current rhythm control therapies in general is that the antiarrhythmic drugs available today are associated with severe side effects. Until safer and

more effective antiarrhythmic drugs have been developed it will not be possible to determine the true potential of the rhythm control strategy.

Proarrhythmia

The ability of the class IA drug quinidine to induce ventricular tachycardia (quinidine syncope) has been known for a long time (Selzer et al., 1964). In 1989, the Cardiac Arrhytmia Supression Trial (CAST) study was stopped due to increased mortality in the patient groups receiving the class IC antiarrhythmic drugs encainide and flecainide. This was the first indication that other classes of antiarrhythmic drugs may also induce serious electrophysiological side effects (1989). It has since been found that not only the class I drugs but also the class III drugs may induce proarrhythmia (Hohnloser et al., 1995).

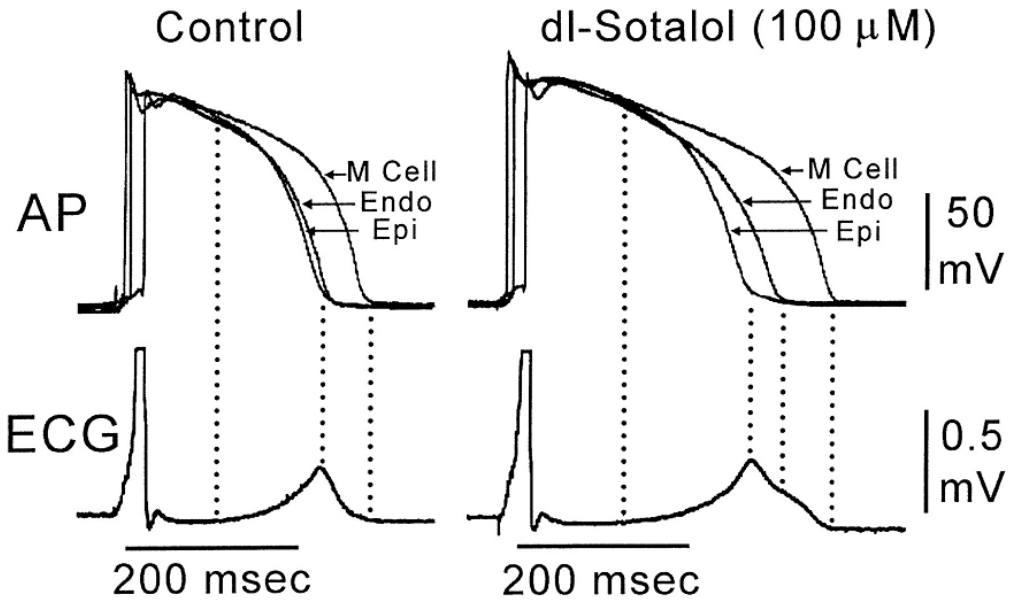

Figure 5. Action potentials recorded in endocardial, midmyocardial (M cell) and epicardial cells in control and following inhibition of IK_r (dl-sotalol) in an isolated perfused canine left ventricular wedge preparation. IK_r inhibition increases the transmural dispersion of ventricular repolarisation, widens the T-wave and prolongs the QT-interval. Modified from Yan et al., 1998; 98:1928-1936 © with permission by Lippincott Williams & Wilkins.

Mechanisms of class III induced proarrhythmia

Class III drugs prolong APD and ERP by inhibition of repolarising potassium currents, preferentially IK_r. The antiarrhythmic action of class III drugs may be attributable to increasing the ERP and hence the wavelength until multiple wavelets can no longer be maintained within the atria (Cosio et al., 2002). Paradoxically, certain conditions of APD prolongation may

result in drug-induced proarrhythmia. As mentioned above, repolarisation in the ventricle is heterogeneous with M cells having longer APD than epi and endocardial cells (Drouin et al., 1995). The long APD in M cells is primarily a consequence of a small IK_s, a prominent late sodium current and a large sodium-calcium exchange current (Zygmunt et al., 2001). Hence, when IK_r is blocked, the APD in M cells is prolonged to a larger extent than the APD in other ventricular cells, leading to increased transmural dispersion of repolarisation and setting the stage for functional reentry (Figure 5) (Yan et al., 1998).

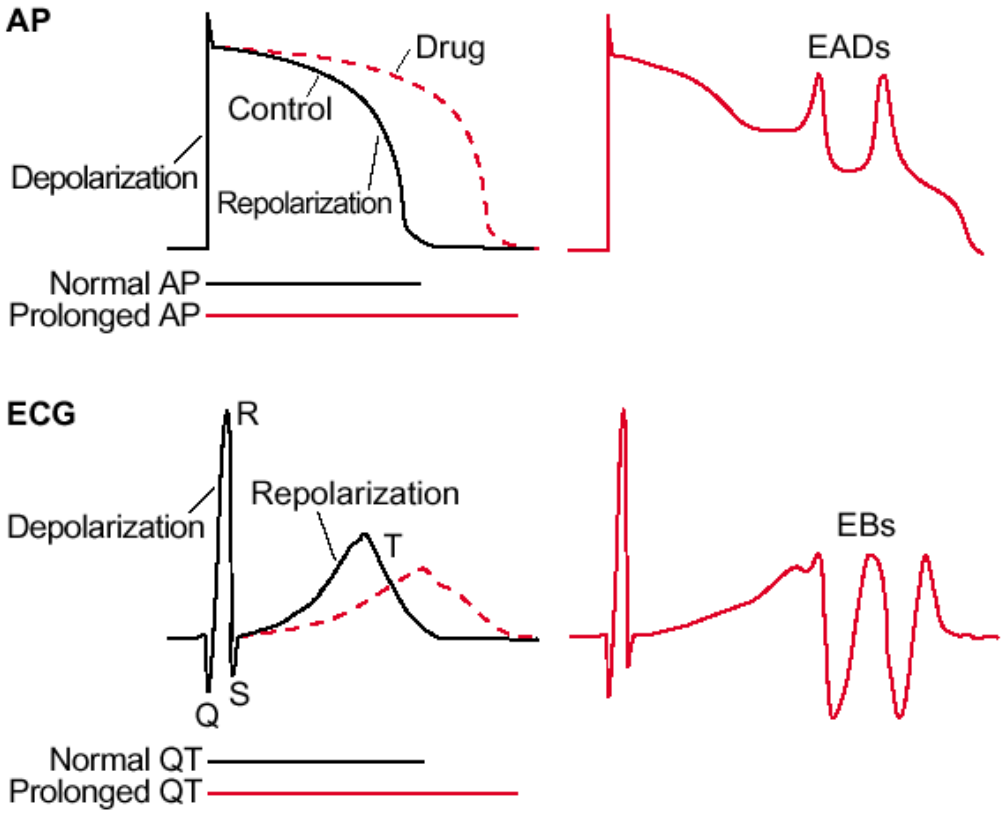

Figure 6. Schematic drawing of a ventricular action potential (AP) and its correlation to the ECG in the control situation (black lines) and following inhibition of IK_r (red lines). Inhibition of IK_r induces prolongation of the action potential duration and the QT-interval, leading to development of early afterdepolarisations (EADs) and ectopic beats (EBs). Reprinted from TRENDS in Pharmacological Sciences, Vol.24, Belardinelli et al. Assessing predictors of drug-induced Torsades de Pointes, p619-625, copyright 2003, with permission by Elsevier.

In addition, the extensive prolongation of APD in M cells and Purkinje cells may promote EADs that may trigger ectopic beats (Figure 6) (Belardinelli et al., 2003). EADs are secondary depolarisations occurring during the plateau (phase 2) and the final repolarisation (phase 3) of the action potential. EADs are thought to be generated by the recovery and reactivation of ICa_L (window Ca^{2+} current) and / or the late sodium current

as a result of incomplete inactivation of sodium channels during the prolonged APD (Volders et al., 2000; Zeng et al., 1995). The combination of an increased dispersion of repolarisation creating a substrate for reentry and EADs triggering reactivation of non-refractory tissue may lead to functional reentry and Torsades de Pointes (TdP) (Antzelevitch et al., 2006; Yan et al., 2001). The term 'Torsades de Pointes', which in English means 'twisting of the points', was originally coined by Desertenne in 1966 as a description of the irregular change in polarity of the QRS complexes of the surface ECG during tachycardia (Desertenne, 1966). Torsades de Pointes may self terminate or aggravate into ventricular fibrillation and sudden death. Risk factors for developing TdP include female gender, hypokalemia, bradycardia and QT prolongation at baseline (Cheng, 2006; Roden, 2004).

Drug-induced long QT syndrome (LQTS) is often referred to as acquired LQTS as opposed to congenital LQTS, which is the result of mutations in genes encoding for various ion channel subunits or anchoring proteins (Nattel et al., 2006).

AZD7009

In light of the increased awareness of poor efficacy and proarrhythmia liability of existing antiarrhythmic agents, AZD7009 was developed in an attempt to find an effective and safe antiarrhythmic drug for treatment of AF. Some important features of AZD7009 are described in the sections below.

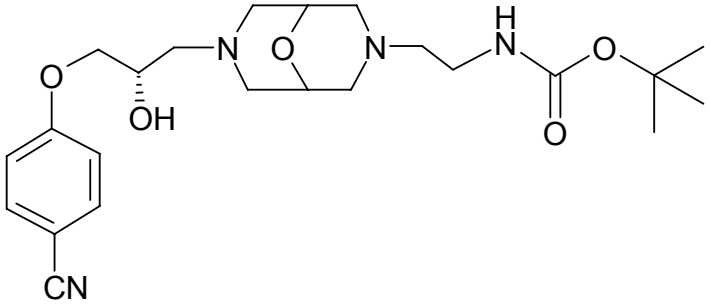

Figure 7. Chemical structure of AZD7009

Electrophysiological characteristics

The differential effect of AZD7009 on atrial and ventricular tissue has been demonstrated in dogs *in vivo* and *in vitro* (Carlsson et al., 2006; Goldstein et al., 2004). AZD7009 concentration-dependently increased the AERP while the effects on the VERP and the QT interval were small. In dog atrial

in vitro preparations, AZD7009 concentration-dependently prolonged APD_{90} and reduced Vmax; the reduction of Vmax was frequency dependent with a larger reduction at higher frequencies whereas the prolongation of the APD_{90} was not. Consistent with the *in vivo* findings, AZD7009 predominantly increased AERP, with only small, dose-independent and frequency-neutral effects on the VERP (Carlsson et al., 2006). In the canine sterile pericarditis model of AF and atrial flutter, AZD7009 increased AERP and VERP by 33% and 17%, respectively, and the QT interval by 9%. In addition, the atrial conduction time was increased more than the ventricular conduction time after exposure to AZD7009 (Goldstein et al., 2004). In dogs with pacing-induced AF and remodelled atria, AZD7009 increased AERP significantly more than VERP (Duker et al., 2005). The predominant effect on AERP and the bell-shaped increase in VERP have been verified in a clinical study in patients undergoing invasive electrophysiological investigation for paroxysmal supraventricular tachycardia (Edvardsson et al., 2005).

Receptor binding assays of AZD7009 have been made for the sodium channel and the L-type calcium channel from rat cerebral cortex. The binding of AZD7009 to the L-type calcium channel depended on the binding site. No inhibition was seen at the dihydropyridine site, whereas the IC_{50} was 5.5 μM for binding to the diltiazem site and 6.6 μM for binding to the verapamil site. The binding of AZD7009 to the sodium channel varied depending on the binding site, with no binding to the tetrodotoxin site and an IC_{50} of 4.3 μM for the veratridine site (AstraZeneca data on file).

The effects of low concentrations (0.2, 0.6 and 1.8 μM) of AZD7009 were studied on I_{to}, IK_s, IK_r, IK_1, INa and ICa_L in acutely isolated dog atrial myocytes. Only IK_r was significantly inhibited by AZD7009, 44% inhibition at 0.6 μM and 69% inhibition at 1.8 μM. The effects of a higher concentration (10 μM) AZD7009 was also studied on INa; 10 μM AZD7009 significantly inhibited INa by 27% at a stimulation frequency of 0.1 Hz. INa was studied at 16 °C and all other currents at 35 °C (AstraZeneca data on file).

In human atrial myocytes, acutely isolated from the right atrial appendage, AZD7009 inhibited I_{to} and IK_{ur} with IC_{50} values of 34 μM and 28 μM, respectively. The recordings were made at 32 to 34 °C, 0.1 Hz. When the stimulation frequency was increased to 3 Hz, the amount of inhibition of I_{to} was slightly increased whereas the amount of inhibition of IK_{ur} was not changed (AstraZeneca data on file).

Efficacy

The ability of AZD7009 to terminate AF has been evaluated in several animal studies. In a rabbit *in vitro* model of acutely dilated right atrium, AZD7009 was highly efficacious in preventing inducibility of atrial fibrillation; the inducibility of AF decreased from 80% to 0% of the preparations, and AF was terminated in 6/6 atria (Löfberg et al., 2006). In the canine sterile pericarditis model, AZD7009 effectively terminated 23/23 AF or atrial flutter episodes and prevented reinduction in 19/20 attempts (Goldstein et al., 2004). AZD7009 terminated 23/23 episodes of AF in dogs with pacing-induced AF (Duker et al., 2005). In a recently published clinical study in AF patients, AZD7009 was highly effective in restoring sinus rhythm (Crijns et al., 2006).

Low proarrhythmic potential

AZD7009 was selected as a candidate drug for clinical development based upon its low proarrhythmic potential as assessed in a sensitive preclinical proarrhythmia model (the methoxamine-sensitised rabbit model of TdP) (Carlsson et al., 1990) and was later shown also to possess low proarrhythmic potential in the isolated arterially perfused dog and rabbit left ventricular wedge preparations (Wu et al., 2005). In the ventricular wedge preparation, action potentials were simultaneously recorded from endocardial, midmyocardial and epicardial cells and, in addition, a transmural pseudo ECG were recorded. AZD7009 prolonged the APD in a bell-shaped manner, and the prolongation was homogenous in all three cell types. This resulted in a minimal increase in the transmural dispersion of repolarisation without accompanying repolarisation-related proarrhythmia. A bell-shaped, concentration-dependent QT interval prolongation was also seen in the methoxamine-sensitised rabbit model (Wu et al., 2005). See Carlsson et al. for a discussion of the usefulness in predicting proarrhythmic potential of the methoxamine-sensitised rabbit model and the isolated arterially perfused left ventricular wedge preparations (Carlsson, 2006). AZD7009 has also been shown to display low proarrhythmic potential in man (Crijns et al., 2006).

AIMS

The general aim of the present *in vitro* studies was to elucidate the mechanisms underlying the predominant atrial effects, the high antiarrhythmic efficacy and the low proarrhythmic potential of the antiarrhythmic agent AZD7009.

The specific aims were:

- To investigate the potency and characteristics of AZD7009 block of the human cardiac ion channels hERG, Kir3.1/Kir3.4, Kv4.3/KChIP2.2, Kv1.5, KvLQT1/minK and Nav1.5 expressed in mammalian cells.

- To study the potency of AZD7009 inhibition of the L-type Ca^{2+} current and the late sodium current in acutely isolated rabbit cardiomyocytes.

- To evaluate the effect of AZD7009 in the absence and presence of the selective IK_r blocker E-4031 on APD in rabbit atrial and ventricular tissue and Purkinje fibre.

MATERIALS AND METHODS

Animals (papers III, V)

The studies were approved by the ethics committee for animal research at Göteborg University, Sweden, and were conducted in accordance with Swedish animal care guidelines. The male New Zealand White rabbits (bodyweight 2.1 to 3.5 kg) used for isolation of cardiomyocytes for voltage-clamp studies and for preparation of tissue for transmembrane action potential (TAP) recordings were bred at HB Lidköpings Kaninfarm (Lidköping, Sweden).

Voltage-clamp experiments (papers I-V)

Ion channel studies of an agent aimed for human clinical use are ideally carried out in isolated human cardiomyocytes, since it would eliminate the problem of potential species differences. Unfortunately, there are many problems associated with the use of human cardiomyocytes. It is difficult to get human tissue for the isolation and the tissue is often diseased hearts. In addition, it is very cumbersome to isolate viable cardiomyocytes from a small piece of tissue that cannot be reterogradely perfused with buffer solutions containing enzymes. A way to circumvent the species problem is to express recombinant human ion channels in mammalian cells. There are further advantages in using cell lines, such as the possibility to store frozen cells for years and to maintain growing cells in culture for weeks or even months. In addition, the overexpression of only one or a few ion channel types simplifies the voltage-clamp recordings since specialised buffers and protocols are not needed to inhibit other contaminating currents. However, it should be emphasised that cultured cells are handled under clearly nonphysiological conditions for the ion channels. Various intracellular components such as accessory subunits, phosphatases / kinases and cytoskeleton that normally interact with the ion channels may be missing. In some cases, the currents through the overexpressed α-subunit may not at all resemble the native current recorded in cardiomyocytes. In those cases it is possible to coexpress the α-subunit with the accessory subunits or other α-subunits.

CHO cells, transfection and cell culturing (papers I-IV)

The ion channel sequences and the method for generation of cells expressing the human cardiac ion channels are described in Table 2. For a

more detailed description of the transfection method see the respective papers. The hERG, Kv4.3/KChIP2.2, KvLQT1/minK and Nav1.5 cells were cultured in HAM/nutrient mix F12 with Glutamax-1 (Invitrogen) and the Kv1.5 and Kir3.1/Kir3.4 cells were cultured in DMEM/nutrient mix F12 with Glutamax-1 (Invitrogen) supplemented with 10% foetal bovine serum (Invitrogen). The CHO cells are often used for ion channel expression because of their low endogenous expression of ion channels, their ease of transfection and their high suitability for patch-clamp experiments (Gabriel et al., 1992; Skryma et al., 1994). The parental CHO cell line was initiated from a biopsy of an ovary of an adult Chinese hamster (Puck et al., 1958).

Table 2 Ion channel sequences and transfections

Ion channel	Accession number	Host cell	Vector	Transfection method	Selection	Stability
Nav1.5	AY148488*	CHO K1	pcDNA3.1	Lipofect-amine 2000	neo	stable
Kv4.3/ KChIP2.2	AH009283 AY026328	CHO K1	pGENIRES	Lipofect-amine plus	neo/hygro	stable
Kv1.5	M83254**	EcR-CHO	pIND		hygro	stable
hERG	U04270	CHO K1	pcDNA3.1	CalPhos	hygro	stable
KvLQT1/ minK	U89364 M26685	CHO K1	pGENIRES pIRES	Lipofect-amine 2000	neo/bleo	transient
Kir3.1/ Kir3.4	NM002239 BC069482	CHO-flpin	pIRES	Lipofect-amine 2000	neo/puro	stable

*for exact sequence see paper III
**for exact sequence see paper II

Isolation of cardiomyocytes (papers III, V)

The L-type Ca^{2+} current (paper V) and the late sodium current (paper III) were studied in acutely isolated cardiomyocytes from the rabbit. Cardiomyocytes from rabbits were chosen because this species had previously been used in several *in vivo* and *in vitro* studies of AZD7009 (Carlsson et al., 2004; Löfberg et al., 2006; Wu et al., 2005) and the predominant atrial effect of AZD7009 has been demonstrated both in rabbits and in man (Edvardsson et al., 2005). In addition, it is feasible to use rabbit hearts in a Langendorff experimental set-up with retrograde perfusion through the aorta.

The procedure for isolation of atrial and ventricular myocytes is described below. Before anaesthesia, a needle was placed in a superficial vein in one of the ears and Heparin 1000 IE/kg was given. Following anesthesia (pentobarbital sodium, 60 mg/kg i.v.), the heart was excised and placed in cold oxygenized Ca^{2+}-free Tyrode's solution (A) supplemented with Heparin 5000 IE/L. A few gentle squeezes were then applied to empty the heart of blood. The heart was mounted on a Langendorff apparatus and subsequently retrogradedly perfused through the aorta with 200 ml of warmed (37 °C) Tyrode's solution (A) containing 1 mM Ca^{2+} followed by perfusion with 200 ml Ca^{2+}-free Tyrode's solution (A). Finally, the heart was perfused with Ca^{2+}-free Tyrode's solution (A) containing Collagenase Type 2 140 U/ml (Worthington Biochemical Corporation) and albumin 0.2 mg/ml (Sigma-Aldrich). During the perfusion, $CaCl_2$ was added three times to a final concentration of 0.25, 0.5 and 1 mM. The perfusion time with collagenase Type 2 in Ca^{2+}-free solutions (A) was varied between 9 and 20 minutes and Ca^{2+} was added every 2 to 5 minutes after that, in total 15 to 40 minutes of enzyme perfusion. A 25-min perfusion period (10 min without Ca^{2+} and addition of Ca^{2+} at 5-min intervals) gave an optimum yield of viable ventricular myocytes. Isolation of atrial myocytes to record sodium currents (paper III) was done with a 15-min perfusion (9 min without Ca^{2+} and addition of Ca^{2+} at 2-min intervals). Some of the atrial myocytes were isolated using a K^+-enriched Ca^{2+}-free Tyrode's solution (B) instead of the normal Ca^{2+}-free Tyrode's solution (A) and without addition of Ca^{2+} during the perfusion. After perfusion with Collagenase Type 2, the heart was removed and the right atria or part of the left or right ventricle was cut into small pieces and placed in 1.5 ml of fresh enzyme containing Tyrode's solution (A) with 1 mM $CaCl_2$ in an E-flask in a water bath (37 °C) with magnetic stirring. Ventricular myocytes for recording the sodium current were isolated from papillary muscle and underlying tissue in the right ventricle. Ventricular myocytes for recording the L-type Ca^{2+} current were isolated from the left ventricular apex. The solution containing collagenase was replaced every 2 to 3 minutes; the suspension was transferred to an Eppendorff tube and centrifuged for 30 s at 200 g. The supernatant was removed, and the pellet was resuspended in Tyrode's solution (A) containing albumin 5 mg/ml. Following centrifugation at 200 g for 30 s, the pellet was resuspended in Tyrode's solution (A) with 1 mM $CaCl_2$. The isolated cardiomyocytes were kept at room temperature with 100 % O_2 and cells were used within 12 hours. The yield of viable, Ca-tolerant cardiomyocytes varied considerably from time to time. The compositions of the buffer solutions used for isolation of cardiomyocytes are listed in Table 3.

Table 3 Buffer solutions for isolation of cardiomyocytes

	A Ca^{2+}-free Tyrode's solution	B K^+ enriched Ca^{2+}-free Tyrode's solution
NaCl	140	120
glucose	10	10
hepes	5	5
KCl	5.4	27
$MgCl_2$	1	1
NaH_2PO_4	1	1

pH 7.4 with NaOH

H9c2 cells, cell culturing (paper V)

Expression of functional recombinant channels is difficult owing to the complex subunit composition of the L-type calcium channel and to this time we have not succeeded in expressing a functional L-type calcium current in mammalian cells. The H9c2 cell line was therefore used as an alternative to study the L-type calcium current. The H9c2 cell line is derived from embryonic rat heart and has endogenous expression of several ion channels including L-type Ca^{2+} channels (Hescheler et al., 1991; Kimes et al., 1976). A drawback of the H9c2 cell line is that it originates from the rat and not human and that it has both cardiac (α_{1C}, $Ca_v1.2$) and skeletal (α_{1S}, $Ca_v1.1$) L-type Ca^{2+} channels. Menard and co-workers found that lowering the amount of foetal bovine serum and adding a low concentration of retinoic acid increased the expression of cardiac L-type Ca^{2+} channels and decreased the expression of skeletal L-type Ca^{2+} channels (Menard et al., 1999). Retinoic acid was thus used in the present study to induce differentiation of the H9c2 cells and increase the expression of cardiac L-type Ca^{2+} channels. The H9c2 cells were cultured in DMEM with Glutamax-1, sodium pyruvate, glucose and pyridoxine (Invitrogen), supplemented with 10% foetal bovine serum (Invitrogen). Differentiation was started one day after plating the cells in small Petri dishes. The concentration of foetal bovine serum was reduced to 1%, and 12 nM retinoic acid was added to the culture media. Recordings were made from cells that were differentiated for 6 to 9 days.

Voltage-clamp recordings (papers I-V)

The patch-clamp technique enables measurements of currents through single ionic channels. A key feature is the establishment of a high resistance seal between the glass pipette and the cell membrane, a gigaohm seal. A

gigaohm seal is achieved by gentle suction applied to the interior of the glass pipette that is filled with salt solution connecting the cell to a headstage amplifier via an Ag/AgCl electrode. The high resistance seal ensures that almost all current flows into the glass pipette and very little current leaks out between the membrane and the glass pipette.

The voltage-clamp recordings in the studies presented here were made using the whole-cell configuration in which the current through all ion channels in the cell membrane is recorded simultaneously (Hamill et al., 1981). Whole-cell recordings can be achieved in two different ways, the standard (used for recordings in CHO and H9c2 cells) or the perforated-patch (used for recordings in cardiomyocytes) whole-cell configuration. Standard whole-cell recordings are achieved by rupture of the cell membrane enclosed by the tip of the glass pipette, thereby accessing the interior of the cell. The hole in the membrane is large enough to allow dialysis of the intracellular compartment, and replacement with the pipette solution occurs rapidly. To be sure that the dialysis reached steady-state a couple of minutes was always allowed before the recordings were started. Perforated-patch whole-cell recordings are achieved by adding an ionophore such as amphotericin B to the pipette solution. After establishment of a high resistance seal, the ionophore incorporates into the cell membrane, creating pores in the membrane. The pores are permeable to small ions, thereby creating electrical access to the interior of the cell, but they are impermeable to larger cytosolic components, thereby leaving the intracellular composition largely intact (D'Ambrosio, 2002).

Voltage-clamp recording means that the membrane potential is kept at a defined value (voltage-clamp) by injection of a current with the proper polarity and magnitude. Hence the membrane currents are directly proportional to the membrane conductance, which is determined by the activity of the ion channels in the membrane. The whole-cell single-electrode technique was used in the present studies, i.e. voltage monitoring and current injection was made continuously by the same electrode. A prerequisite for this is to have a series resistance that is small (ideally two orders of magnitude) relative to the cell resistance. For an introduction to the whole-cell voltage-clamp recording technique see (Sontheimer et al., 2002).

Voltage-clamp recordings were made with an EPC9 amplifier (HEKA Elektronik). Glass pipettes were fabricated from thick-walled, filamented, borosilicate glass capillaries (Harvard apparatus Ltd) with an inner and outer diameter of 1.16 and 2 mm (paper I) or 0.86 and 1.5 mm (papers II,

III, IV, V). The glass capillaries were pulled with a micropipette puller, model P-97 (paper I) or P-2000 (papers II, III, IV, V) (Sutter Instruments, USA), and had a resistance of 1 to 5 MΩ (usually 2 to 4 MΩ) when filled with electrode solution. In recordings with the standard whole-cell configuration, the series resistance was kept under 15 MΩ and compensated for by 75-85%. Currents were sampled at 1-100 kHz depending on channel and protocol, for details see the respective papers, and filtered at 2.9 kHz (EPC9 internal 4-pole Bessel filter) using Pulse software v8.53 or v8.63 (HEKA Elektronik, Germany). In the perforated-patch recordings in isolated cardiomyocytes, Amphotericin B (Sigma-Aldrich) was diluted in the pipette solution to a final concentration of 200 μg/ml. Gentle suction was applied to achieve giga-ohm or near giga-ohm seal formation; whole-cell access was established within 20 minutes and the series resistance was compensated for by 50 %. All experiments were carried out at room temperature (22°C) and the holding potential was -80 mV unless otherwise noted. The buffer solutions used for voltage-clamp recordings in CHO cells, H9c2 cells and cardiomyocytes are listed in Table 4.

Table 4 Buffer solutions for voltage-clamp recordings in CHO cells, H9c2 cells and cardiomyocytes

	C EC CHO	D IC CHO	E EC H9c2	F IC H9c2	G EC myo (INa)	H IC myo (INa)	I EC myo (ICa)	J IC myo (ICa)
NaCl	140	10	90	10	140		140	10
glucose	5		5		10		10	
hepes	10	10	10	10	5	10	5	10
Kasp		110						
KCl	5.4	20						
CsCl	1.8			120	5.4	120	5.4	120
$MgCl_2$	1	1	1	1	1	1	1	1
NaH_2PO_4							1	
$CaCl_2$		1			1.8		1.8	
EGTA		10		11		11		11
TEA-Cl				10		10		10
MgATP				5		5		5
K_2ATP		5						
$BaCl_2$			40	1				

C, D, E, G, I pH 7.4 with KOH; H pH 7.2 with CsOH; F, J pH 7.4 with CsOH
myo = cardiomyocyte, Kasp = potassium aspartate
IC = intracellular buffer, EC = extracellular buffer

The extracellular ion concentrations in normal heart ventricle are (in mM): Na^+ 140, K^+ 4, Mg^{2+} 0.6, Ca^{2+} 1.25, Cl^- 140. Inside ventricular cells the ion concentrations are (in mM): Na^+ 20, K^+ 140, Mg^{2+} 17, Ca^{2+} 0.0002-0.001, Cl^- 25 (Opie, 2004). The equilibrium potential of an ion may be calculated from the Nernst equation

$$E_s = \frac{RT}{zF} \ln \frac{[s]_2}{[s]_1} \qquad \text{(Equation 1)}$$

where Es is the equilibrium potential for the ion s, R is the gas constant, T is the absolute temperature, z is the valence of the ion, F is Avogadro's number, $[s]_1$ is the intracellular concentration of the ion s and $[s]_2$ is the extracellular concentration of the ion s. According to the ion concentrations given above for the normal heart ventricle, the equilibrium potential is approximately +52 mV for Na^+, –95 mV for K^+, +95 mV to +117 mV for Ca^{2+} and -46 mV for Cl^-. The resting membrane potential in myocardial cells is close to the equilibrium potential for K^+. This is due to the large membrane permeability to K^+ ions through inwardly rectiying potassium channels, e.g. IK_1.

Cell superfusion system (papers I-V)

Buffer solutions were applied to the cells using two different superfusion systems, a traditional superfusion system (paper I) and the Dynaflow superfusion system (papers I-V) with either 8 or 16-channel chips (Dynaflow™, DF-8 Pro II or DF-16, Cellectricon AB, Sweden) or a prototype chip with 32 channels (Figure 8) (Sinclair et al., 2002). The traditional perfusion system consisted of a RSC-160 rapid solution changer (Biologic, France) and a CMA100 microinjection pump (Carnegie Medicin, Sweden) connected to the recording bath via polyethylene tubing. Cells used in this system were grown on coverslips. During the experiment, a coverslip was placed in the recording bath mounted on an inverted microscope and the recording bath was continuously superfused with extracellular solution. When the Dynaflow superfusion system was used, a suspension of cells was transferred directly into the recording bath of a Dynaflow chip that was mounted on an inverted microscope. The cell suspension was obtained by detaching the cells with a cell scraper or by trypsination. Fluid was driven through the channels using pressurized air supplied to the device via a microinjection pump (CMA100), producing a laminar liquid stream of solutions at the channel outlets. In order to apply solutions to the voltage-clamped cell, the cell was lifted up and positioned in front of the channel outlet of interest. The widths of the channels were

50 µM in the 16-channel chip and 150 µM in the 8-channel chip. Since the dimensions of the cardiomyocytes were of the magnitude of 100 µM, three consecutive channels were used for each concentration of drug when the 16-channel chip was used.

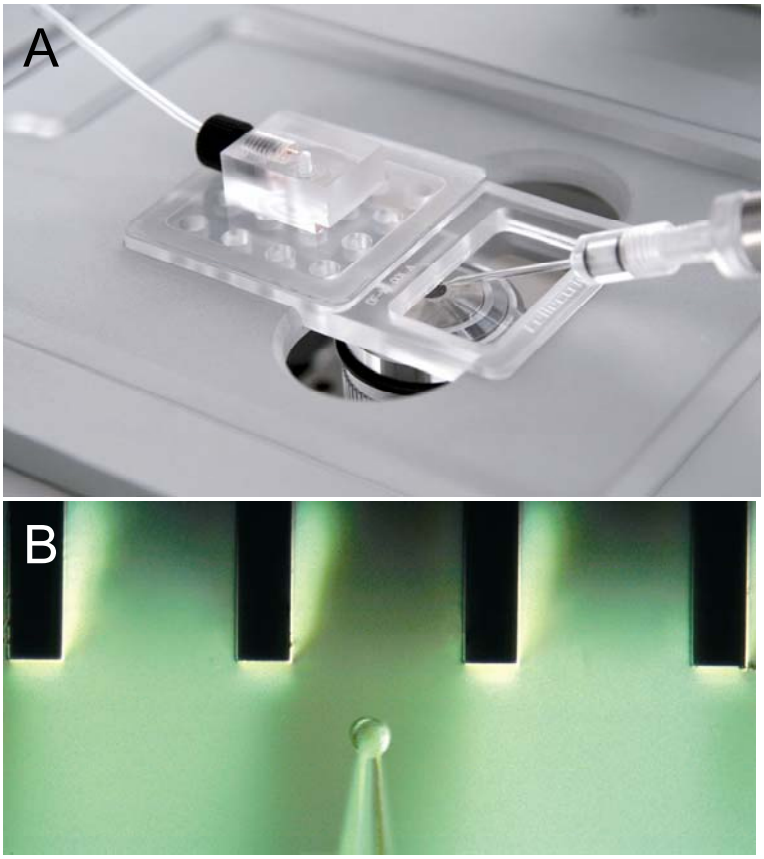

Figure 8. A. A Dynaflow™ DF-16 chip mounted on an inverted microscope. The glass patch pipette is placed in the recording bath. B. A magnification of the patch pipette with a cell attached to its tip. The patch pipette is placed in front of one of the micro channel outlets. With permission from Cellectricon AB, Sweden.

Pulse protocols (papers I-V)

Current through individual ion channels is always of an all or none character; the channels are either closed or inactivated nonconducting or open conducting. The current recorded using the whole-cell configuration is, as mentioned above, the total of the current through all ion channels in the cell membrane. Hence, the whole-cell current is governed by the statistical probability of the individual ion channels being conducting or nonconducting. Since every cell contains many ion channels, the openings of the individual channels are not seen. The current rather seems to activate, inactivate and deactivate in a smooth, continuous way. The single channel conductances of the ion channels used in the present studies are 2 pS to 40 pS depending on the type of ion channel and the intra and extracellular

concentrations of the conducting ion. Hence the whole cell currents measured are the sum of the current through a couple of hundred to a couple of thousand ion channels. Certain voltage pulse protocols are used to be able to describe the characteristics of the whole-cell currents and their blockade or activation by different drugs (Carmeliet et al., 1998). The section below describes the voltage pulse protocols used in this thesis; see the respective papers for greater detail.

Activation, inactivation and deactivation (papers I, II, III, V)

The current is often activated using a square pulse protocol from the repolarised holding potential to a depolarised potential. During the square pulse, the current increases until the maximal current is reached (activation), declines upon continued depolarisation (inactivation) and then decreases upon return to repolarised or resting potentials (deactivation). The largest current during a square pulse stimulation is called the peak current. It is sometimes more feasible to measure the current amplitude at a time point after the peak current; this is called the late, sustained or steady-state current e.g. Kv1.5. Another alternative is to measure the current-time integral, the area under the curve (AUC) e.g. Kv4.3. It is also common to measure the current amplitude during a repolarising step after the square pulse stimulation; this is called the tail current e.g. hERG.

The rate of current activation is characteristic for the specific ion channels. Some ion channels activate very rapidly, e.g. Nav1.5, and some activate very slowly, e.g. KvLQT1/minK. The rate of activation may be quantified by estimating the time constant of activation (τ_{act}) from an exponential curve fit to the rising phase of the current. τ_{act} is usually voltage dependent and faster at higher depolarising potentials.

In a similar manner, the rate of inactivation can be quantified by an exponential curve fit to the decaying phase of the current; multiple exponentials are often needed to obtain a good fit. The time constant(s) of inactivation (τ_{inact}) are therefore often referred to as the fast and slow time constants of inactivation. Similar to the rate of activation, the rate of inactivation is often faster at increasing potentials.

The rate of deactivation may be estimated by an exponential curve fit to the decaying phase of the tail current. During exposure to certain drugs, a tail current crossover may be seen when the tail current recorded in control conditions and the tail current recorded during exposure to a drug are superimposed (Franqueza et al., 1998; Snyders et al., 1992). A tail current crossover is seen for drugs that block the ion channel in the open state and

prevent closing of the channel while the drug is still bound. During a block by such an open channel blocker, the peak amplitude of the tail current will be smaller and the rate of deactivation will be slower, leading to the tail current crossover. The slower rate of deactivation may be explained by the extra time needed for the drug molecule to leave the binding site upon return to repolarised potentials. When the drug molecule leaves the ion channel it is still in an open state and some current will pass before the ion channel finally closes.

Current-voltage curves (papers I, II, V)

The potential at which activation starts and the potential at which maximum activation is reached are characteristic features for the different voltage activated ion channels; these parameters can easily be seen in a current-voltage (I-V) plot. Activation protocols are created with a stepwise increase in the voltage of the square pulse to more and more depolarised potentials to be able to construct I-V plots where the current amplitude at different activating potentials is plotted versus the potential of the activating pulse. Since the ion channels studied have varying activation kinetics, activation protocols with different potential intervals and pulse duration were used for the various ion channels, see Table 5.

Table 5 Current-voltage protocols

	Activating potential (mV)	Tail current potential (mV)	Pulse duration (ms)
Nav1.5	-80 to +40	no	30
Kv4.3/KChIP2.2	-80 to +60	no	1000
Kv1.5	-60 to +60	-40	300+200
hERG	-60 to +50	-60	4000+4000
ICa_L (cardiomyocytes)	-40 to +30	no	400

The current (I) is determined by the conductance (G) of the ion channels and the driving force. The conductance is determined by the number of open conducting channels and the single channel conductance of the specific ion channel. The driving force is determined by the difference between the actual potential (*Vm*) and the reversal potential (*Vrev*) for the specific ion. Vrev can be calculated from equation 1. Thus the current can be described by

$$I = G(V_m - V_{rev}) \qquad \text{(equation 2)}$$

If the conductance is calculated and plotted versus the applied potential, the potential for half-maximal activation (V_{50}) may be estimated from a fit of the resulting conductance-voltage curve to a Boltzmann sigmoidal function

$$Y = \min + (\max - \min)/(1 + \exp((V_{50} - V_m)/slope)) \quad \text{(equation 3)}$$

In order to use equation 2 for calculation of ion channel conductance, the I-V relation is assumed to be linearly related to the driving force. However, for many types of K^+-channels, the I-V relation has a nonlinear dependence upon the driving force. To get a more accurate determination of the G-V relation of K^+ channels, the following equation may be used:

$$I_K \approx g_K(V,t)V\{\exp(q(V - E_K)/kT) - 1\}/\{\exp(qV/KT) - 1\} \text{ (equation 4)}$$

where I_K is the potassium current, g_K is the potassium conductance, E_K is the reversal potential for potassium, q is the unit electronic charge, k is the Boltzmann constant and T is the absolute temperature, derived from the Goldman-Hodgkin-Katz current equation (Clay, 2000). Equation 4 was used to construct G-V relations for Kv1.5 and Kv4.3/KChIP2.2.

The current through sodium channels may be described by equation 4 if recorded in Ca^{2+}-free conditions. However, extracellular Ca^{2+} ions block sodium currents in a voltage-dependent manner that obscures the applicability of equation 4 (Clay, 2000). In the present studies of the cardiac sodium current, Ca^{2+} was present in the extracellular buffer solutions and equation 4 was therefore not used to construct I-V relations. Conduction was instead calculated according to equation 2.

When tail currents recorded at a fixed repolarised potential are used as a measure of the amount of activated current, the problem of normalizing currents from different potentials is avoided because the driving force is constant throughout the measurements. Hence, the I-V relation does not have to be corrected for driving force and the V_{50} may be directly determined from the I-V plot. This was the case for the hERG currents.

Steady-state inactivation curves (papers I, II)

Steady-state inactivation curves or availability curves estimate the fraction of ion channels that are available for activation at different potentials. Steady-state inactivation curves are constructed by increasing the potential during a prepulse given immediately before the activating pulse. The current during the activating pulse is normalised to the largest current

recorded and plotted versus the potential of the prepulse. The potential for half-maximal inactivation or availability (V_{50}) may be estimated by a fit of the resulting curve with a Boltzmann sigmoidal function (equation 3). The steady-state inactivation protocols used for the different ion channels are shown in Table 6.

Table 6 Steady-state inactivation protocols

	Prepulse potential (mV)	Activating potential (mV)	Prepulse duration (ms)
Nav1.5	-130 to -20	-10	2000
Kv4.3/KChIP2.2	-120 to +20	+40	6000
Kv1.5	-120 to +20	+20	6000

Concentration dependence of block (papers I-V)

The concentration-effect curves for block by AZD7009 and reference compounds were determined by exposing cells to increasing drug concentrations; four to eight concentrations between 0.01 and 1000 μM were used. The duration of exposure to each drug concentration depended upon both the type of ion channel and the drug examined. Following exposure to the drug, the current was allowed to stabilize at the new level (steady-state) before the next concentration of the drug was applied. The pulse protocols used and the duration of exposure to each concentration of AZD7009 for the different ion channels are listed in Table 7. Concentration-effect curves were constructed by plotting the current normalised to that in control conditions versus the logarithm of drug concentration. An estimate of the concentration for half-maximal inhibition (IC_{50}) was obtained by curve fit to the experimental data. A sigmoidal dose-response curve with variable slope was used.

$$Y = \min + (\max - \min)/(1 + \exp((\log IC_{50} - X)Hillslope)) \quad \text{(equation 5)}$$

where X is the logarithm of the concentration and Y is the normalised current.

Table 7 Concentration-response protocols

	Activating potential (mV)	Pulse duration (ms)	Frequency (Hz)	Time of exposure to AZD7009 (min)	Measured current
Nav1.5	-10	30	0.2/10	3	peak
Nav1.5 (late)	-10	300	0.2	3	late[c]
Kv4.3/KChIP2.2	+40	1000	0.2	3.3	AUC
Kv1.5	+20	300	0.2	3	ss
hERG	+20/-60[a]	2000/2000	0.1	5	tail
KvLQT1/minK	+40	6000	0.05	3	ss
Kir3.1/Kir3.4	-80[b]	70000		1.2	ss
ICa_L (H9c2)	+20	500	0.1	5	peak
ICa_L (myo)	0	400	0.1	5	peak
INa (myo)	-10	300	0.2	3	late[c]

a, tail current
b, Kir3.1/Kir3.4 current was activated by addition of 70 mM K^+
c, late sodium current was measured between 200 and 220 ms after the start of depolarisation
ss = steady-state
myo = cardiomyocytes

Time course of block (papers I, II)

When a drug accesses the binding site in an ion channel only after channel activation, the development of the block will be visible if it is slower than the activation process but fast enough to develop during the activating pulse. Hence, during a square pulse activation of the current, the time constant of the block (τ_{block}) may be estimated from an exponential curve fit to the decaying phase of the current. If the current inactivates under control conditions, the inactivation process must also be considered.

If the time constant of the block is determined at two or more concentrations, an estimate of the apparent association (*k*) and dissociation (*l*) rate constants can be made from a linear fit of the inverse of τ_{block} plotted versus the concentration according to equation 6 (Snyders et al., 1992).

$$1/\tau_{block} = k \times [D] + l \quad \text{(equation 6)}$$

Assuming a bimolecular reaction, the apparent K_D can be calculated from the association and dissociation rate constants according to equation 7.

$$K_D = l/k \quad \text{(equation 7)}$$

Association and dissociation rate constants were calculated for the AZD7009 block of hERG, Kv1.5 and Kv4.3/KChIP2.2 current.

Different ways of estimating τ_{block} were used for the different ion channels because of the differences in inactivation kinetics. Kv4.3/KChIP2.2 inactivates rapidly with a double exponential time course; the relative contribution of τ_{fast} is larger than τ_{slow}. During exposure to AZD7009, the apparent rate of inactivation was increased due to a more rapid τ_{fast} and an increase in the relative contribution of τ_{fast} (Table 2, paper II). The time constant of the block was calculated using an approximation of the channel-blocking kinetics by AZD7009 according to the equation:

$$1/\tau_{decay} = 1/\tau_{block} + 1/\tau_{inactivation} \qquad \text{(equation 8)}$$

$\tau_{inactivation}$ was approximated by τ_{fast} in the absence of AZD7009 and τ_{decay} was approximated by τ_{fast} in the presence of AZD7009 (Hatano et al., 2003).

Kv1.5 inactivates with a mono-exponential time course in the absence of the drug. In the presence of AZD7009 the current declined with a double exponential time course; τ_{fast} was concentration dependent whereas τ_{slow} was independent of the concentration, and the magnitude of τ_{slow} was not significantly different from $\tau_{inactivation}$ in the absence of the drug. Hence, τ_{fast} was considered to represent τ_{block}. The time constant of the block of the hERG current was determined by a mono-exponential curve fit to the difference between the current recorded in control conditions and the current recorded during exposure to AZD7009.

Use- and frequency-dependence of drug block (papers I, II, III)

Use- and frequency-dependent block are common features of many ion channel blocking drugs. Use-dependence of the block refers to the ability of the block to develop only after activation of the ion channel, i.e. the drug has a higher affinity for activated or inactivated states than for the rested state. Frequency-dependence of the block is the case in which the amount of inhibition of an ion current at steady-state varies with the stimulation frequency (Carmeliet et al., 1998).

The use-dependence of the AZD7009 block of hERG, Kv1.5, Kv4.3/KChIP2.2 and Nav1.5 was evaluated using a protocol in which AZD7009 was added while holding the membrane potential at a repolarised potential where all ion channels reside in the closed state. After a sufficient

duration for reaching the steady-state block during repetitive pulse stimulation, activation of the current was started. If closed channels were blocked by AZD7009, steady-state block would already be present at the first stimulating pulse, whereas, if closed channels were not blocked by AZD7009, no inhibition would be present at first and inhibition would increase as the stimulating pulses continued. Similar protocols were also used to study whether washout of the effect of AZD7009 was dependent on the activation, i.e. use-dependence of unblock.

The frequency-dependence of the block was studied by changing the stimulation frequency during steady-state block to see whether the amount of block differed at differing stimulation frequencies. Late sodium currents in isolated rabbit atrial and ventricular myocytes and peak and late sodium currents in CHO K1 Nav1.5 cells were studied using frequency changes between 0.1 and 1 Hz (paper III). The peak sodium current in CHO K1 Nav1.5 cells was studied during frequency changes between 0.2 and 10 Hz (paper I) and Kv1.5 and Kv4.3/KChIP2.2 currents were studied during frequency changes between 0.2 and 5 Hz (paper II).

Recovery from inactivation and use-dependent block (paper I)

Recovery from inactivation can be determined by a double pulse protocol separated with a variable interpulse interval at a repolarised potential. During the first activating pulse, the current activates and inactivates; during the interpulse interval, the current recovers from inactivation to various extents depending on the duration of the interpulse interval. Recovery from inactivation and use-dependent block by AZD7009 was determined for Nav1.5 using a protocol with 30 ms activating pulses to -10 mV, and an interpulse interval at -110 mV of varying duration (0.3 ms to 600 s).

Prepulse potentiation (paper I)

The hERG current recorded in the presence of AZD7009 was increased at potentials between –60 and –30 mV, i.e. at potentials near the threshold for activation. Prepulse-dependent agonistic effects have previously been described for azimilide (Jiang et al., 1999) and almokalant (Carmeliet, 1993). To test if the agonistic effect of AZD7009 was also prepulse-dependent, the following protocol slightly modified from Jiang et al. was used. The hERG current was activated by repetitive pulses to -30 mV and the amount of block by AZD7009 was determined. When steady-state was reached, one highly depolarised pulse to +40 mV was

applied, followed again by repetitive pulses to –30 mV. The same protocol was also executed in the absence of the drug.

Fractional electric distance (paper II)

The voltage dependence of the block at potentials more positive than needed for maximal activation of the ion channels reflects the influence of the transmembrane electric field on the interaction between the binding site and a charged drug molecule. When the relative current $I_{drug}/I_{control}$ is plotted versus the activating potential, a curve fit to the relative current at potentials more positive than needed for maximal activation yields an estimate of the fractional electric distance (δ) of the binding site from the inside, according to the equation

$$1-\left([D]/\left([D]+K_D^{*}\cdot e^{-z\delta FE/RT}\right)\right) \qquad \text{(equation 9)}$$

where [D] is the concentration of the drug, K_D^{*} is an estimate of the K_D at the reference potential 0, E is the clamp step potential, δ is the fractional electric distance, z is the valence (+1 for cationic AZD7009), F is the Faraday constant, R is the gas constant and T is the absolute temperature (Woodhull, 1973). It should be noted that the electric distance is not interchangeable with the physical distance. AZD7009 has a pKa of 9.7 and hence >99% of the drug molecules will be charged at pH 7.4. The fractional electric distance was calculated for the AZD7009 block of Kv1.5 and Kv4.3/KChIP2.2.

Currents in isolated cardiomyocytes (papers III, V)

In voltage-clamp recordings the focus is usually on one ion current at a time. Hence, when ion currents are recorded in isolated cardiomyocytes the ion current of interest must be isolated from the other ion currents that are present in the cardiomyocyte. This is usually done by ion substitution, addition of specific pharmacological agents and/or specialised voltage pulse protocols designed to isolate the current of interest. The cardiac sodium current and the L-type calcium current were studied in separate experiments. In order to inhibit contaminating potassium currents, recordings of both INa and ICa_L were made using CsCl instead of KCl in the pipette and bath solutions. In addition, tetra ethyl ammonium (TEA), which inhibits potassium currents, was added to the pipette solution.

Recordings of INa were made in the presence of 5 μM nifedipine to inhibit ICa_L. The magnitude of the late sodium current in isolated cardiomyocytes

is very small; in rabbit isolated ventricular and atrial myocytes it was 0.2 pA/pF, giving a whole cell current of 15 to 20 pA (paper III). Measuring currents that small is difficult and 10 nM ATX-II (anemonia sulcata toxin) was thus used to amplify the late sodium current. ATX-II has been proposed to enhance the late sodium current by prolonging the channel open time, facilitating channel opening from the closed state and preventing complete inactivation (Schreibmayer et al., 1987). In addition, ATX-II prolongs the APD and induces EADs in rabbit ventricular myocytes (Studenik et al., 2001). Sodium currents were activated using 300 ms pulses to -10 mV at a stimulus frequency of 0.2 Hz. The late sodium current was measured as the mean current in the window between 200 and 220 ms from the start of the depolarisation, and the current recorded following addition of 100 μM TTX was used as the zero current level. Furthermore, in atrial myocytes, a simplified action potential pulse of a 100-ms step to +20 mV followed by a 100-ms ramp back to -80 mV and finally 100 ms at –80 mV was used (modified from (Clancy et al., 2003)).

Recordings of ICa_L were undertaken immediately after a 20-ms long prepulse to -40 mV that inhibited the sodium current. Calcium currents were activated using 400 ms pulses to 0 mV at a stimulation frequency of 0.1 Hz. The peak calcium current was quantified as the difference between the peak current and the current at the end of the 400 ms pulse.

Transmembrane action potential recordings (paper III)

Transmembrane action potentials were recorded in single cells from a small piece of tissue in an *in vitro* set-up, which enables recording of action potentials for up to several hours.

Male New Zealand White rabbits were anaesthetised with pentobarbital sodium (60 mg/kg i.v.). The heart was cut out and placed in potassium-enriched Tyrode's solution (L) in order to stop spontaneous contractions. Tissue pieces approximately 5x15 mm in size were taken from the right atrial auricle or the right ventricle (anterior papillary muscle with Purkinje fibres running across its base). The Purkinje fibre preparation included a piece of ventricular tissue which rendered the preparation more stable and decreased spontaneous activity. The piece of tissue was mounted in an organ bath (2 ml) continuously superfused with 37°C Tyrode's solution (K). The compositions of the buffer solutions used in the transmembrane action potential recordings are listed in Table 8.

Table 8 Buffer solutions for transmembrane action potential recordings

	K Tyrode's solution	L Potassium enriched Tyrode's solution
NaCl	130	131
glucose	5.5	55
KCl	4	27
$NaHCO_3$	18	18
$CaCl_2$	1.8	2.5
NaH_2PO_4	1.8	0.9
$MgSO_4$	0.5	
$MgCl_2$		0.5

The buffer solutions were gassed with a mixture of 5% CO_2 and 95% O_2 to maintain a pH of 7.4.

The preparation was stimulated at a basic cycle length of 500 ms (pulses 2 ms in duration and 100% above threshold in intensity) via a pair of Ag/AgCl electrodes mounted in the floor of the organ bath and connected to a stimulator (stimulus isolator A385, World Precision Instruments, UK). A stabilization period of two hours was allowed before the experimental protocol was started, during which the tissue was continuously stimulated at the basic cycle length. A microelectrode filled with 3 M KCl (resistance 15 to 20 MΩ) connected via an Ag/AgCl junction to a high impedance amplifier (Intracellular Electrometer IE-210, Warner Instrument Corporation, USA) was used for the transmembrane action potential recordings. The set-up allowed recording from two microelectrodes simultaneously, i.e. action potentials from ventricular tissue and Purkinje fibre were recorded simultaneously from the same piece of tissue. The same impalement was kept as long as possible but the signal deteriorated a times and the microelectrode had to be moved to a neighbouring cell. Since cells in the close vicinity have similar electrical properties, it is justified to record action potentials from several different cells during one experiment. A recording of action potentials at the basic cycle length of 500 ms (2 Hz) was made after approximately 30 min at each concentration of the drug(s) when the steady-state effect of the drug had been reached. At the steady-state level, data from a 5-sec period were saved on manual command (sampling frequency 20 kHz). The different action potential characteristics were analysed using custom-designed software (PharmLab v5.0b4, AstraZeneca). The 50% and 90% levels of action potential repolarisation (APD_{50} and APD_{90}) were calculated on the average of ten consecutive action potentials. Following recordings at the basic cycle length, the interstimulus interval

between consecutive action potentials was increased in 2-ms steps up to a final cycle length of 1000 ms in order to provoke EADs. All action potentials were continuously recorded during this time period (sampling frequency 1 kHz).

Statistical analysis

Data are given as mean ± SEM. Statistical differences were tested with one- or two-way ANOVA. When statistical differences were found, individual differences were evaluated using Bonferroni's, Dunnett's or Tukey's multiple comparison post test, and paired or unpaired Student's t-test, as appropriate. Differences between data sets were considered statistically significant at $p<0.05$. Pulsefit (HEKA Elektronik) and Igor Pro (Wavemetrics Inc.) were used for analyses of current amplitudes and exponential curve fit in voltage-clamp recordings. Microsoft Excel (Microsoft) and GraphPad Prism (GraphPad Software) were used for data processing and statistical analysis.

RESULTS

Effects of AZD7009 on ion channels expressed in CHO cells

The section below describes the details of AZD7009 block individually for each ion channel. A summary of the effects on ion channels expressed in CHO cells is given at the end.

hERG current (paper I)

A representative recording of hERG current during inhibition by AZD7009 is shown in Figure 9.

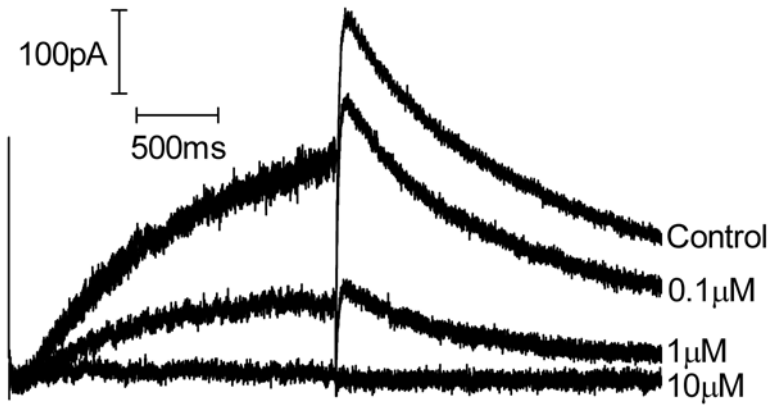

Figure 9. Recording of AZD7009 inhibition of hERG current in CHO K1 cells. Currents were activated by 2 s depolarising pulses to +20 mV, and 2 s tail currents were recorded at -60 mV. The stimulation frequency was 0.1 Hz.

Inhibition of hERG current in CHO K1 cells was concentration dependent, with an IC_{50} of 0.6 ± 0.1 μM (n=6, Table 9). The time constant of the block (τ_{block}) was determined by mono-exponential fit to the difference between the control current and the current following exposure to 1 μM (τ_{block}= 2.72 ± 0.76 s) and 15 μM (τ_{block}= 216.8 ± 43.6 s) AZD7009. The apparent association and dissociation rate constants were determined according to equation 6; *k* was 0.33 μM^{-1} s^{-1} and *l* was 0.15 s^{-1}. According to equation 7, the K_D was 0.45 μM, which is close to the experimentally determined IC_{50} value. When washin of 1 μM AZD7009 was done without stimulating pulses, the current during the first activating pulse was initially

not blocked, but the block developed during the square pulse activation and reached steady-state within a few stimulations. The current was still blocked when stimulations were recommenced following washout of AZD7009 during quiescence. The potential for half maximal activation was -8.2 ± 0.1 mV under control conditions and was significantly shifted in the repolarising direction following exposure to 1 μM AZD7009, -18.0 ± 0.6 mV (n=14, p<0.001). AZD7009 induced prepulse potentiation of the hERG current at near threshold potentials. The current directly following a prepulse to +40 mV was increased by 281 ± 40% and the prepulse potentiation declined with a time constant of 46.5 ± 12.5 s, n=4.

Nav1.5 current (papers I, III)

Inhibition of the cardiac sodium current was dependent upon AZD7009 concentration and stimulation frequency. In CHO K1 cells stably expressing Nav1.5, the IC_{50} was 7.9 ± 1.5 μM (n=5) at 0.2 Hz stimulation and 4.3 ± 1.2 μM (n=6) at 10 Hz stimulation (Table 9).

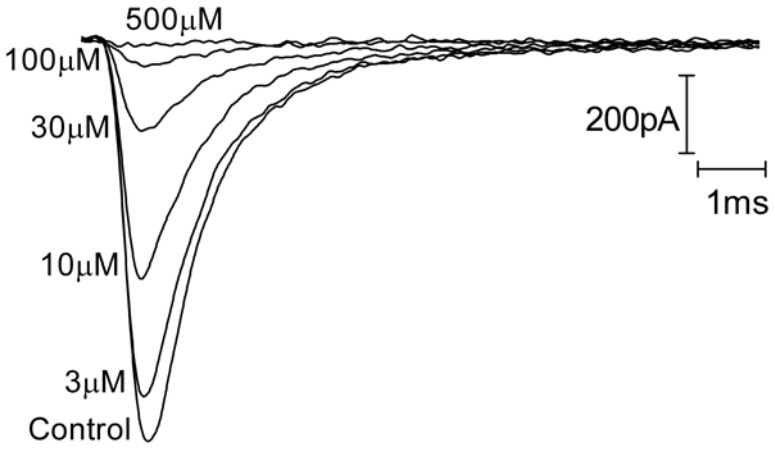

Figure 10. Representative recording of AZD7009 inhibition of Nav1.5 current in CHO K1 cells. Currents were recorded by 30-ms depolarising pulses to –10 mV at 0.2 Hz.

A representative recording of Nav1.5 current during block by AZD7009 is shown in Figure 10. In separate experiments, the amount of block during exposure to 10 μM AZD7009 was significantly larger at 10 Hz than 0.2 Hz stimulation. Activation of the hNav1.5 current was needed in order for a block by 10 μM AZD7009 to develop, but unblock during washout was not dependent on channel activation. Neither the time needed to reach 50% of the maximal peak current amplitude nor the time constants of inactivation

were significantly changed by 10 μM AZD7009. The potential for half maximal activation was not significantly changed during exposure to 10 μM AZD7009; V_{50} was -24.1 ± 0.5 mV under control conditions and -25.9 ± 0.5 mV during exposure to AZD7009 (n=7). The potential for half maximal availability was -68.8 ± 0.9 mV under control conditions and -74.9 ± 0.6 mV during exposure to 10 μM AZD7009 (n=6). The change was not significantly different from the shift seen in time-matched control measurements. In the absence and presence of 10 μM AZD7009, recovery from inactivation of hNav1.5 was best described by a double exponential function.

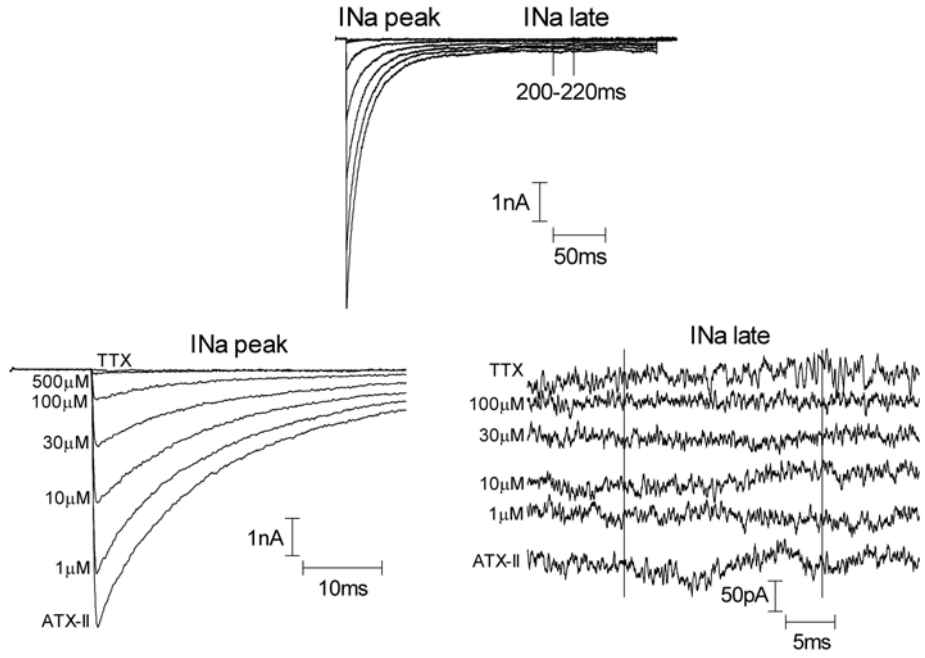

Figure 11. Sodium currents in CHO cells recorded in the presence of ATX-II and increasing concentrations of AZD7009. The bottom panel shows magnifications of the peak sodium current (left) and the late sodium current (right). The late sodium current was measured as the mean current in the window between 200 and 220 ms (lines) from the start of the depolarisation, and the current recorded following addition of 100 μM TTX was used as the zero current level.

In the absence of AZD7009, >80% of the current recovered within 10 ms, consistent with a rapid recovery from inactivation of Nav1.5 channels. In the presence of AZD7009, approximately 20% of the current, corresponding to the unblocked hNav1.5 channels, recovered rapidly, whereas a large component of the current, corresponding to the blocked hNav1.5 channels, recovered very slowly.

The late sodium current recorded in the presence of 10 nM ATX-II was inhibited, with an IC_{50} of 11 ± 2 μM (n=6, Table 9) (Figure 11). Inhibition of the late sodium current by 10 μM AZD7009 was more pronounced at 1 Hz stimulation than at 0.1 Hz stimulation.

Kv4.3/KChIP2.2 current (paper II)

A representative recording of the Kv4.3/KChIP2.2 current during block by AZD7009 is shown in Figure 12.

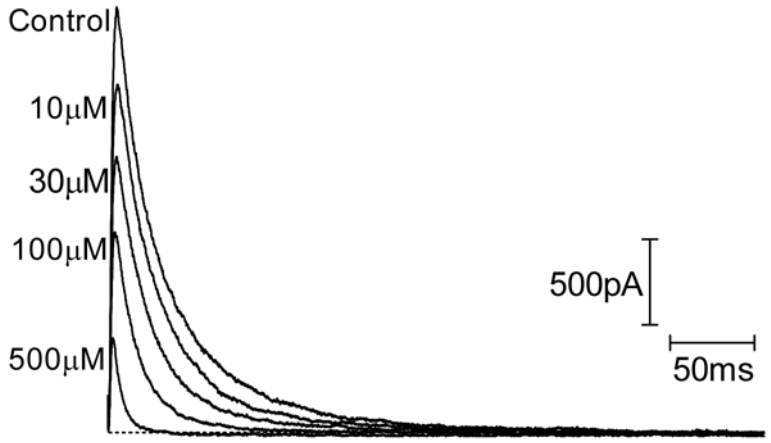

Figure 12. Original recordings of Kv4.3/KChIP2.2 current in CHO K1 cells exposed to increasing concentrations of AZD7009. Currents were recorded by 1-s depolarising pulses to +40 mV at 0.2 Hz.

Inhibition of the hKv4.3/hKChIP2.2 current in CHO K1 cells was concentration and frequency dependent; the IC_{50} was 23.7 ± 4.4 μM (n=5, Table 9) at 0.2 Hz stimulation. In separate experiments, the amount of block during exposure to 25 μM AZD7009 was significantly more pronounced at 5 Hz (76 to 78% block) than at 0.2 Hz (60% block) stimulation ($P<0.001$, n=7). During washin of 25 μM AZD7009 without stimulating pulses, inhibition was seen at the first stimulating pulse and unblock during washout occurred without stimulations. The association (*k*) and dissociation (*l*) rate constants were estimated by linear regression according to equation 6; *k* was 0.33 ± 0.02 μM^{-1} s^{-1} and *l* was 11.2 ± 5.9 s^{-1}. According to equation 7, the K_D was 33.6 μM, which is reasonably close to the experimentally determined IC_{50} value. The potential for half maximal activation was not significantly changed during exposure to 25 μM AZD7009; V_{50} was -5.7 ± 0.9 mV under control conditions and -6.4 ± 0.8 mV during exposure

to AZD7009 (n=7). The potential for half maximal availability was -39.8 ± 0.6 mV under control conditions and -43.9 ± 1.1 mV during exposure to 25 μM AZD7009 (n=7). V_{50} was not significantly different in washout experiments. The fractional electric distance (δ) calculated according to equation 9 was 0.32.

Kv1.5 current (paper II)

Inhibition of the Kv1.5 current was concentration dependent with an IC_{50} of 27.0 ± 1.6 μM (n=6, Table 9) at 0.2 Hz stimulation. A representative recording of the Kv1.5 current during inhibition by AZD7009 is shown in Figure 13.

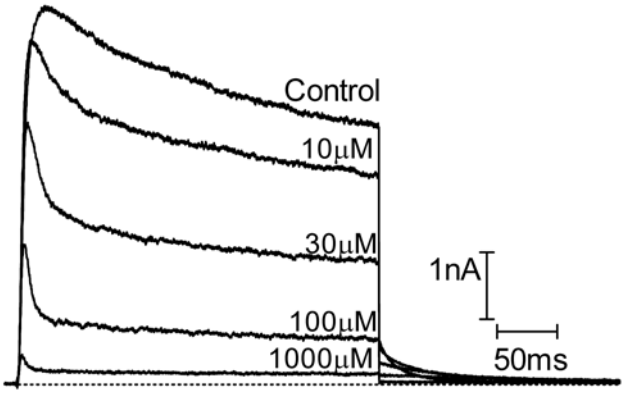

Figure 13. Representative recording of Kv1.5 current in CHO cells exposed to increasing concentrations of AZD7009. Kv1.5 currents were activated by 300-ms depolarising pulses to +20 mV at 0.2 Hz.

During exposure to 25 μM AZD7009, the stimulation frequency was changed between 0.2 and 5 Hz. The amount of block was significantly increased during 0.2 Hz (54% block) as compared to 5 Hz (41 to 44% block) stimulation ($P<0.05$, n=5), i.e. there was a reverse frequency dependence. During washin of 25 μM AZD7009 without stimulating pulses, inhibition was seen at the first stimulating pulse and unblock during washout occurred without stimulations. In the presence of AZD7009, the amplitude of the tail current was decreased in a concentration dependent way and the tail current deactivation was slowed, causing tail current crossover. A significant decrease in the tail current amplitude was seen at 3 μM and higher concentrations. The association (*k*) and dissociation (*l*) rate constants were estimated by linear regression according to equation 6; *k* was 1.3 ± 0.1 μM^{-1} s^{-1} and *l* was 36.8 ± 3.2 s^{-1}. According to equation 7, the

K_D was 27.7 μM, which is very close to the experimentally determined IC_{50} value. The potential for half maximal activation was -9.6 ± 2.0 mV under control conditions and -15.6 ± 2.7 mV during exposure to AZD7009 (n=5). The change was not significantly different from time-matched control measurements. The potential for half maximal availability was -17.9 ± 1.9 mV under control conditions and was not significantly changed during exposure to 25 μM AZD7009 -20.0 ± 2.1 mV (n=7). The fractional electric distance (δ) calculated according to equation 9 was 0.20.

Kir3.1/Kir3.4 current (paper IV)

Inhibition of Kir3.1/Kir3.4 current expressed in CHO cells was concentration dependent with an IC_{50} of 166 ± 44 μM (n=7, Table 9). A representative recording of the Kir3.1/Kir3.4 current during block by AZD7009 is shown in Figure 14.

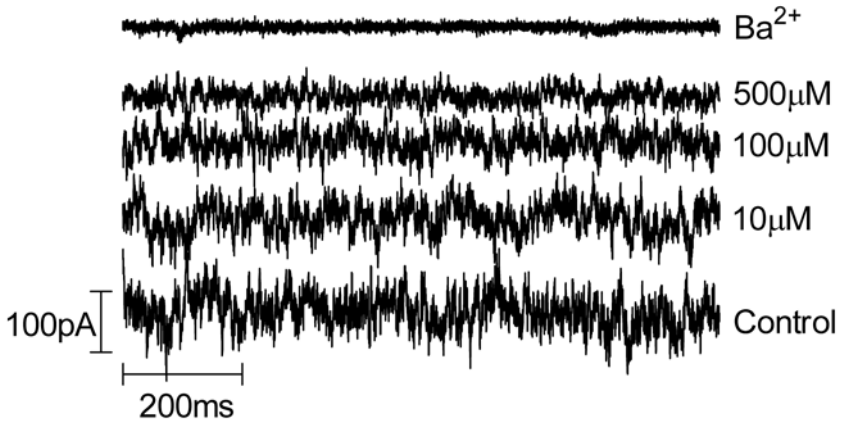

Figure 14. AZD7009 inhibited the Kir3.1/Kir3.4 current in CHO cells in a concentration dependent way. Currents were stimulated by addition of 70 mM KCl. The current recorded in the presence of 3 mM $BaCl_2$, a concentration that totally inhibits the Kir3.1/Kir3.4 current, was used as the zero current level.

KvLQT1/minK current (paper I)

Inhibition of KvLQT1/minK current transiently expressed in CHO K1 cells was concentration dependent with an IC_{50} of 193 ± 20 μM (n=6, Table 9). A representative recording of KvLQT1/minK current during block by AZD7009 is shown in Figure 15.

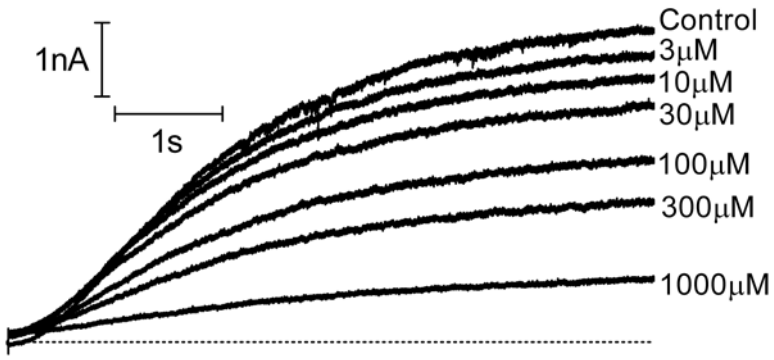

Figure 15. Representative recording of the KvLQT1/minK current in CHO K1 cells exposed to increasing concentrations of AZD7009. Currents were recorded by 6-s depolarising pulses to +40 mV at 0.05 Hz.

Summary of effects of AZD7009 on ion channels in CHO cells

A summary of the concentration and frequency dependent inhibition of the ion currents is given in Figure 16 and Table 9.

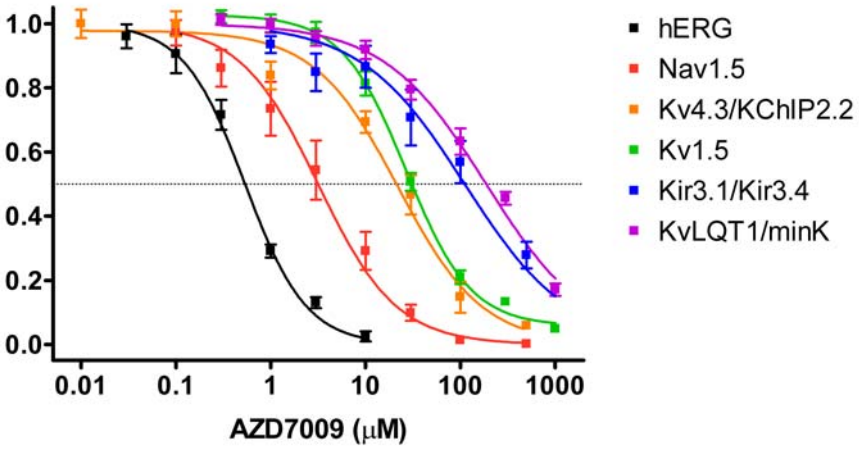

Figure 16. Concentration-response relationships for inhibition of hERG, Nav1.5 (10 Hz), Kv4.3/KChIP2.2, Kv1.5, Kir3.1/Kir3.4 and KvLQT1/minK by AZD7009.

Table 9 Concentration response for AZD7009

	IC_{50} (μM)	Hill slope	Frequency (Hz)	n
Nav1.5 peak	7.9 ± 1.5	1.40 ± 0.08	0.2	5
	4.3 ± 1.2	1.05 ± 0.09	10	6
Nav1.5 late	11 ±2 μM	1.0 ± 0.2	0.2	6
Kv4.3/KChIP2.2	23.7 ± 4.4	0.98 ± 0.12	0.2	5
Kv1.5	27.0 ± 1.6	1.28 ± 0.10	0.2	6
hERG	0.6 ± 0.1	1.34 ± 0.16	0.1	6
KvLQT1/minK	193 ± 20	0.81 ± 0.05	0.05	6
Kir3.1/Kir3.4	166 ± 44	0.79 ± 0.09		7

Activation and inactivation kinetics are presented in Table 10 and Table 11 and the major ion channel-blocking characteristics are summarised in Table 12.

Table 10 Activation kinetics

	Activation start (mV)	Activation max (mV)	V_{50} (mV) control	V_{50} (mV) AZD7009[a]
Nav1.5	-40	0	-24.1 ± 0.5	ns
Kv4.3/KChIP2.2	-20	+20	–5.7 ± 0.9	ns
Kv1.5	-30	+10	-9.6 ± 2.0	ns
hERG	-40	+20	-8.2 ± 0.1	-18.0 ± 0.6*

AZD7009 concentration was 10 μM for Nav1.5, 25 μM for Kv4.3/KChIP2.2 and Kv1.5 and 1 μM for hERG
ns=no significant change following exposure to AZD7009
*$p<0.001$ versus V_{50} control

Table 11 Inactivation kinetics

	V_{50} (mV) control	V_{50} (mV) AZD7009[a]
Nav1.5	–68.8 ± 0.9	ns
Kv4.3/KChIP2.2	-39.8 ± 0.6	ns
Kv1.5	-17.9 ± 1.9	ns

a, the AZD7009 concentration was 10 μM for Nav1.5 and 25 μM for Kv4.3/KChIP2.2 and Kv1.5
ns=no significant change following exposure to AZD7009

Table 12 Summary of ion channel block by AZD7009

	Nav1.5	Kv4.3/ KChIP2.2	Kv1.5	hERG	KvLQT1/ minK	Kir3.1/ Kir3.4
IC_{50} (μM)	4.3[a]	24	27	0.6	193	166
Frequency dependence	yes	yes	yes (reverse)			
I-V	ne	ne	ne	hyp		
Activation (τ)	ne	faster	faster	faster		
Inactivation (τ)	ne	'faster'[b]	'faster'[b]			
Deactivation (τ)			slower	ne		
Block after activation	yes	yes	yes	yes		
Trapping	no	no	no	yes		
Prepulse potentiation				yes		

a, 10 Hz
b, development of block, not faster inactivation *per se*
ne = no effect
hyp = hyperpolarised

Currents in isolated cardiomyocytes

Late sodium current (paper III)

In isolated rabbit cardiomyocytes, AZD7009 concentration-dependently inhibited the late sodium current. A representative recording of the late sodium current in a rabbit atrial myocyte following exposure to ATX-II and AZD7009 is shown in Figure 17.

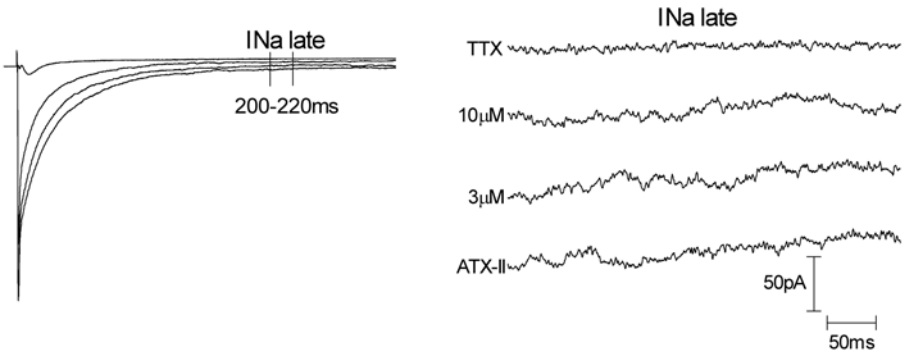

Figure 17. Inhibition of the late sodium current in an isolated rabbit atrial myocyte. Currents were recorded in the presence of ATX-II 10 nM alone and in combination with 3 μM and 10 μM AZD7009. TTX (100 μM) was used as the zero current level. The right panel shows a magnification of the late sodium current.

AZD7009 at 3 μM and 10 μM inhibited the late sodium current by 22±4% and 53±4% in ventricular myocytes (n=6) and 20±3% and 54±1% in atrial myocytes (n=5), respectively. The amount of block did not differ significantly between ventricular and atrial myocytes. In accordance, lidocaine at 25 μM inhibited the late sodium current in both atrial and ventricular cells. The amount of block by AZD7009 and lidocaine in atrial myocytes using the simplified action potential pulse protocol was not significantly different from the amount of block observed with the standard pulse protocol.

L-type calcium current (paper V)

AZD7009 inhibited the L-type calcium current in acutely isolated rabbit cardiomyocytes with an IC_{50} of 91±30 μM at a stimulation frequency of 0.1 Hz, n=4. Representative recordings in control conditions and during exposure to increasing concentrations of AZD7009 are shown in Figure 18.

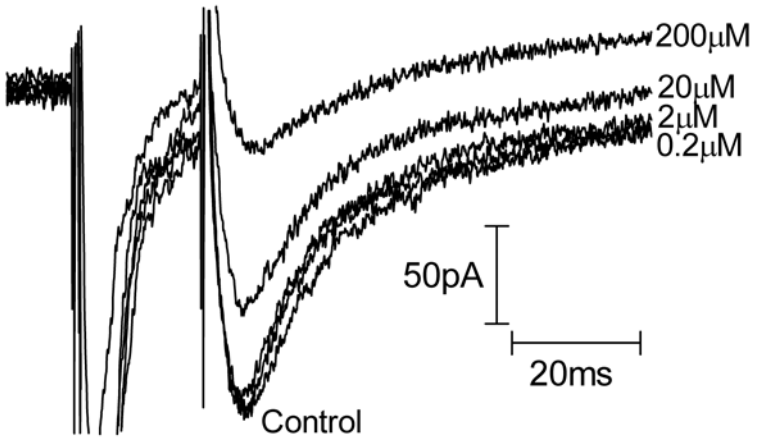

Figure 18. Recordings of the L-type Ca^{2+} current in rabbit isolated ventricular myocytes in control conditions and following exposure to increasing concentrations of AZD7009.

L-type calcium current in H9c2 cells (paper V)

The L-type Ca^{2+} currents in H9c2 cells, recorded with Ba^{2+} as the charge carrier, were concentration-dependently inhibited by AZD7009. The IC_{50} was 17 ± 6 μM and the Hill slope was 0.9 ± 0.1, n=5. Representative recordings of the L-type Ca^{2+} current during exposure to increasing concentrations of AZD7009 are shown in Figure 19.

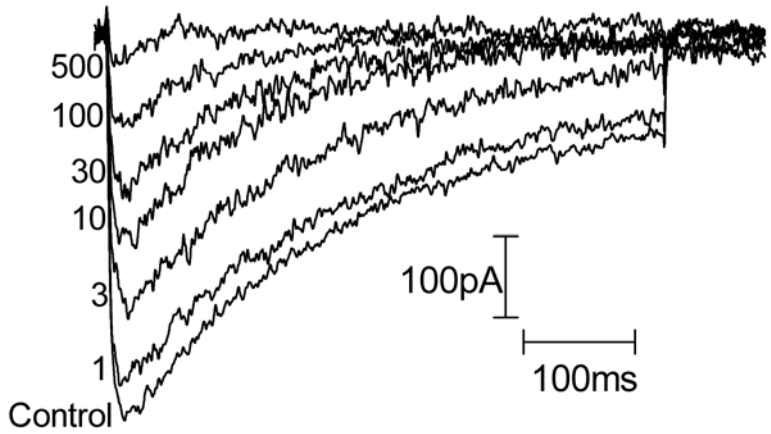

Figure 19. AZD7009 concentration-dependently inhibited the L-type calcium current in H9c2 cells. Currents were activated by 500-ms depolarisations to +20 mV at 0.1 Hz and Ba^{2+} was used as the charge carrier.

Transmembrane action potentials (paper III)

Transmembrane action potentials were recorded in atrial and ventricular tissue and in Purkinje fibre during exposure to AZD7009 and the selective IK_r blocker E-4031. The study included three different series of experiments. In the first series, 3 and 10 μM AZD7009 were added alone and thereafter 5 μM E-4031 was added to the superfusate containing 10 μM AZD7009. In the second series of experiments, 5 μM E-4031 was first added alone and an addition of AZD7009 of 3 and 10 μM was then made. Lidocaine was given in combination with E-4031 in a third series of experiments. The basic cycle length was 500 ms. The APD_{90} results are summarised in Figure 20. In the first series of experiments, the low concentration of AZD7009 alone induced a significant prolongation of APD_{90} in all cell types; a significant prolongation of APD_{50} was seen only in ventricular tissue. The high concentration of AZD7009 significantly prolonged APD_{90} in all tissue types and APD_{50} in ventricular and atrial tissue. An addition of E-4031 in combination with AZD7009 did not further prolong the APD in any tissue. In the second series of experiments, E-4031 at 5 μM significantly prolonged APD_{90} in all cell types and APD_{50} in ventricular tissue and Purkinje fibre. The addition of AZD7009 in combination to E-4031 produced varying results in the different cell types. Adding AZD7009 in combination with E-4031 significantly attenuated the APD prolongation caused by E-4031 in Purkinje fibre, but not in the ventricle. In contrast, in atrial tissue, the addition of AZD7009 in

combination with E-4031 further prolonged the APD. The APD prolongation induced by the combination of 10 μM AZD7009 and 5 μM E-4031 was not significantly dependent on the sequential order of the addition of the drugs.

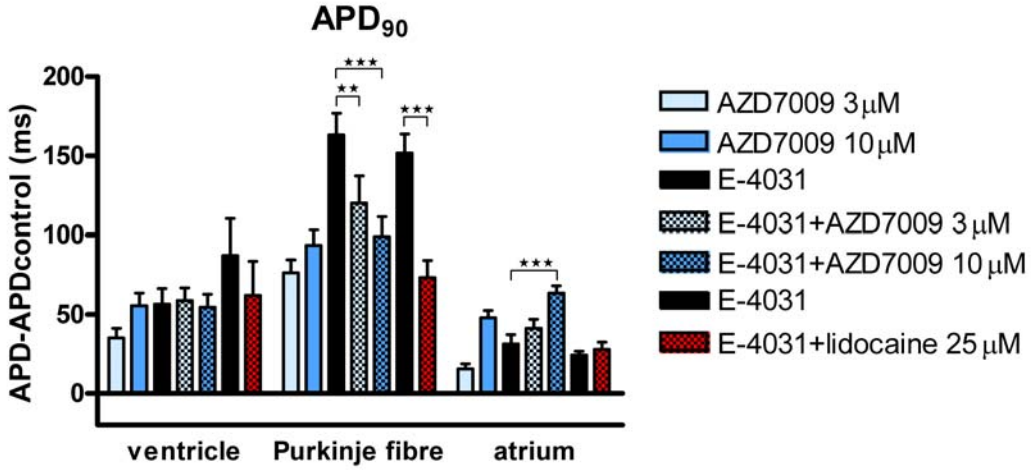

Figure 20. A summary of the effects on APD_{90} of AZD7009 alone and E-4031 alone and in combination with either AZD7009 or lidocaine. The effect is expressed as the change (in ms) in APD_{90} from baseline, i.e. predrug. The significance level of the change in APD_{90} following addition of AZD7009 or lidocaine to the E-4031-superfused preparations is indicated, **$p<0.01$, ***$p<0.001$, n=6-7.

For comparision, separate experiments were carried out with 25 μM lidocaine added in combination with E-4031. This combination of lidocaine and E-4031 significantly attenuated the APD prolongation in Purkinje fibre. In atrial and ventricular tissue, however, the addition of lidocaine in combination with E-4031 did not significantly change the APD (Figure 20).

When the cycle length was increased in steps of 2 ms up to 1000 ms, EADs were induced by 5 μM E-4031. An addition of 10 μM AZD7009 (n=4) or 25 μM lidocaine (n=4) attenuated the E-4031-induced APD prolongation and suppressed the E-4031-induced early afterdepolarisations in all preparations.

GENERAL DISCUSSION

Characteristics of ion channel blockade by AZD7009

All the three cardiac potassium channels that were thoroughly investigated, Kv4.3/KChIP2.2, Kv1.5 and hERG, seem to be blocked by AZD7009 through the same basic mechanism (papesr I and II). Channel activation was needed for the block to develop, indicating that the binding site of AZD7009 is located such that drug access is permitted in the open state only.

During washout, AZD7009 was trapped in the hERG channel and activation of the channel was needed for the unblock of AZD7009 to occur. Trapping drug molecules in closed hERG channels is a well known feature of several hERG-blocking drugs, e.g. dofetilide and almokalant (Carmeliet, 1992; Carmeliet, 1993). The phenomenon has been explained by the trapping of the drug molecule in the inner vestibule of the hERG channel following closure of the activation gate (Mitcheson et al., 2000). However, no trapping of AZD7009 occurs in Kv4.3/KChIP2.2 or Kv1.5 channels. This may be explained by differences in the size of the inner vestibule of the channels, with the hERG channel having a larger inner vestibule that allows closure of the activation gate with the drug molecule still bound, whereas closure of the activation gates in the other channels occurs only after dissociation of the drug molecule. The hypothesis that AZD7009 must leave the channel before it can close is supported by data on Kv1.5 block, where AZD7009 slows the rate of deactivation and induces a tail current crossover. The rate of deactivation of hERG is not slowed by AZD7009, which is consistent with the trapping of AZD7009 in closed hERG channels.

In Kv4.3/KChIP2.2 and Kv1.5 channels, AZD7009 does not block the peak current to the same extent as the steady-state current. This may be explained by the necessity of channel opening before the drug molecule can bind to and block the channel. The block develops during the prolonged depolarisation, and it appears as though AZD7009 accelerates the inactivation process of the current, but the reason is actually the development of block and not faster inactivation *per se*. Since the drug molecule must leave the channel before it can close, the same procedure of block and unblock occurs during each cycle of depolarisation and repolarisation. The steep voltage dependence of the block of Kv4.3/KChIP2.2 and Kv1.5 current occurring at potentials between -30 and

0 mV overlaps with the voltage dependence of activation of the currents, consistent with an open channel block.

The IC_{50} values for the block of hERG (0.6 μM), Kv4.3/KChIP2.2 (24 μM) and Kv1.5 (27 μM) by AZD7009 correlate well with the potency obtained for inhibition of IK_r in isolated dog atrial myocytes (44% inhibition at 0.6 μM) and for inhibition of I_{to} and IK_{ur} in isolated human atrial myocytes (IC_{50} values of 34 μM and 28 μM, respectively). The IC_{50} value for inhibition of the peak sodium current by AZD7009 in CHO Nav1.5 cells (7.8 μM) is close to that obtained for inhibition of the peak sodium current in isolated dog atrial myocytes (27% inhibition at 10 μM), especially considering the lower stimulation frequency and temperature in the dog atrial myocytes (0.1 Hz and 16 °C) compared to that in CHO Nav1.5 cells (0.2 Hz and 22 °C).

Similar to the block of the potassium channels, the block of the Nav1.5 channel was dependent on channel activation. However, AZD7009 did not influence the rate of activation or inactivation of the Nav1.5 current, indicating that the process of block development was slower than the rate of activation and inactivation of the Nav1.5 current. A likely explanation is that AZD7009 binds to and inhibits the Nav1.5 channel in its inactivated state and that channel opening is required for the drug molecule to access the binding site. A similar block mechanism has been described for flecainide, which, like AZD7009, has a high pKa and is thus charged to a large extent at physiologic pH (Liu et al., 2003; Liu et al., 2002).

Unblock of AZD7009 during washout did occur without channel activation, but the unblocking process was very slow, with a time constant of 131 s. The amount of block increased following increases in the stimulation frequency. Since the rate of recovery from block upon return to a lower frequency was faster ($\tau = 37.8$ s) than the rate of unblock with no stimulations, it is likely that unblocking to a large part, although probably not exclusively, also occurs through open Nav1.5 channels. It should be noted that all voltage-clamp recordings in the present studies were made at room temperature. Johns et al. noted that recovery from block by O-demethyl-encainide (a metabolite of encainide) was markedly increased at higher recording temperature (Johns et al., 1989). Hence, it can not be excluded that the recovery from block by AZD7009 is changed at a higher and more physiological temperature.

The frequency-dependent block by AZD7009 of the cardiac sodium current is also evident in recordings of the maximum phase 0 upstroke velocity

(Vmax) of action potentials recorded in dog atrial tissue at 35°C (Carlsson et al., 2006). In that study it was noted that, following steady-state block of AZD7009, premature activations did not further reduce Vmax, suggesting that the recovery from the block of the sodium channel was also slow at more physiological conditions, i.e. in accordance with the slow time constant of the unblock of Nav1.5 channels reported in paper I.

The late and the peak sodium current recorded in CHO Nav1.5 cells in the presence of ATX-II was inhibited with a similar potency by AZD7009; the IC_{50} values were 11 μM and 16 μM, respectively. The late sodium current recorded in acutely isolated atrial and ventricular myocytes was also inhibited with similar potency, an approximately 50% block at 10 μM AZD7009. Inhibition of the late sodium current has been described for several agents such as lidocaine (Fedida et al., 2006; Orth et al., 2006), flecainide (Fedida et al., 2006; Nagatomo et al., 2000), RSD1235 (Fedida et al., 2006; Orth et al., 2006), ranolazine (Antzelevitch et al., 2004; Belardinelli et al., 2006) and amiodarone (Maltsev et al., 2001). The reported amounts of inhibition of the late sodium current relative to the peak sodium current are different for the various drugs. Ranolazine inhibits the late sodium current considerably more (a 30-fold difference) than the peak sodium current, and similar results are found for amiodarone and lidocaine (10-fold difference). In contrast, flecainide and RSD1235 inhibit both currents to a similar extent. A larger inhibition of the late than the peak sodium current would theoretically create favourable repolarisation and cardioprotective effects (see discussion below) in the absence of conduction effects. For AZD7009, inhibiting both the peak and the late sodium currents with similar potency, both repolarisation and conduction will be affected.

AZD7009 inhibited ICa_L in isolated rabbit ventricular myocytes with low potency, the IC_{50} being 91 μM at 0.1 Hz stimulation frequency. The potency of the block of ICa_L carried by Ba^{2+} ions in H9c2 cells was higher, the IC_{50} here being 17 μM. In receptor binding assays of ICa_L from rat cerebral cortex, the IC_{50} was 5 to 6 μM. These discrepancies in the amount of inhibition of ICa_L by AZD7009, which may be related to species differences or differences in the experimental conditions, make it difficult to predict the potency of AZD7009 inhibition of ICa_L.

It should also be noted that the effects of AZD7009 on several other important cardiac ion currents, such as ICa_T, I_f and ion transporters, e.g. the sodium-calcium exchange current, have not yet been investigated. A role in the mechanism of action of AZD7009 for those currents can currently not

be ruled out, but the major effects of AZD7009 are most likely attributed to the combined inhibition of IK_r, INa, IK_{ur} and I_{to}.

Mechanisms underlying the predominant atrial effects of AZD7009

The predominant action of AZD7009 on atrial electrophysiological variables has been described in several animal models (Carlsson et al., 2006; Duker et al., 2005; Duker et al., 2004; Goldstein et al., 2004) and in man (Edvardsson et al., 2005). The work reported in paper III examined the change in APD in atrial tissue during exposure to 5 μM E-4031, a concentration that totally and selectivly inhibits IK_r, and during exposure to a combination of E-4031 and AZD7009. The APD prolongation in atrial tissue, but not in ventricular tissue, was larger during exposure to the combination of E-4031 and AZD7009 than during exposure to E-4031 alone. When lidocaine, a selective sodium current blocker, was added together with E-4031, it did not influence the change in the atrial APD caused by E-4031. Hence, AZD7009 further increased the atrial APD via mechanisms that are separate from the inhibition of IK_r and INa. These additive effects indicate that atrial-selective repolarising currents are in fact inhibited and functionally important even at relatively low concentrations of AZD7009.

The prolongation of the atrial APD was already pronounced at the lowest concentration of AZD7009 (3 μM), and there is most likely a minor degree of block of the early repolarising currents (IK_{ur} and I_{to}) acting in synergy with the more prominent inhibition of IK_r that adds to the predominant atrial action. Since the potency of AZD7009 inhibition of Kir3.1/Kir3.4 (IK_{ACh}) (investigated in paper IV) is very low, it is not likely that inhibition of IK_{ACh} contributes to the prolongation of the atrial APD. Interestingly, in electrically remodeled goat atria, administration of the compound AVE0118 (which predominantly inhibits I_{to}, IK_{ur} and IK_{ACh} (Gögelein et al., 2004)) synergistically increased AERP and the AF conversion rate when combined with a selective IK_r blocker (Blaauw et al., 2003; Brendel et al., 2004), suggesting a synergistic action of the inhibition of IK_r and the more atrial selective currents I_{to}, IK_{ur} and IK_{ACh}.

Another important factor that may add to atrial selectivity is the inhibition of the late sodium current that counteracts the ventricular APD prolongation induced by inhibition of IK_r (paper III). A more pronounced prolongation of atrial APD may arise since the impact of late sodium current blockade may

be larger in some ventricular cells, e.g. the M cells, and in Purkinje fibre cells than in atrial cells; see the discussion below.

The difference in prolongation of the APD in ventricular and atrial cells by AZD7009 would hence be determined by both an increased atrial APD prolongation due to the synergistic inhibition of IK_r, I_{to} and the atrial specific IK_{ur} in atrial cells and a decreased ventricular APD prolongation due to the larger impact of late sodium current inhibition on ventricular cells.

Mechanisms underlying the high antiarrhythmic efficacy of AZD7009

The antiarrhythmic efficacy of AZD7009 may be attributed to the combined inhibition of repolarising potassium currents (IK_r, I_{to} and IK_{ur}) and the cardiac sodium current, leading to a prolonged APD and an increased ERP that increases the reentrant wavelength. A prolonged wavelength would reduce the number of reentrant circuits that can be harboured within the atria and, according to the multiple wavelet theory, the AF would hence destabilize and finally terminate. However, the impact of sodium current inhibition on antiarrhythmic efficacy is complex because, in addition to increasing the ERP, it also decreases the conduction velocity. This latter effect would then shorten the reentrant wavelength and consequently attenuate the antiarrhythmic efficacy or, in areas of slow conduction, eventually lead to termination of atrial fibrillation when the reentrant wavefront is blocked. In the canine sterile pericardities model, such a block of the reentrant wavefront by AZD7009 was seen in a region of slow conduction (Goldstein et al., 2004).

A role of decreased conduction velocity in terminating AF has been described in a goat model of AF (Wijffels et al., 2000). Wijffels and coworkers found that a widening of the excitable gap (i.e. the difference between the AF cycle length and AERP) between the reentrant wavelets was correlated to the termination of AF by class I drugs. Their explanation was that widening of the excitable gap would favour fusion of wavelets and improve recovery of excitability, and that the decreased number of fibrillating wavelets would lead to termination of AF. If the conduction effects of AZD7009 contribute to the antiarrhythmic action of the drug, this would add to the atrial selectivity since AZD7009 has been reported to have a greater effect on conduction in the atria than in the ventricles (Goldstein et al., 2004).

Mechanisms underlying the low proarrhythmic potential of AZD7009

Unlike the case of the conventional class III drugs, i.e. pure IK_r blockers, the APD prolongation induced by AZD7009 in the ventricle seems to be associated with a low risk of repolarisation-related proarrhythmia (Wu et al., 2005). The low proarrhythmic potential of AZD7009 is most likely attributable to the inhibition of the late sodium current, with an uncertain extent of contribution of the inhibition of the L-type calcium current (see the discussion of ICa_L below). Following exposure to AZD7009, the APD will increase as a consequence of the inhibition of IK_r, but an excessive APD prolongation in M cells and Purkinje cells is counteracted by the inhibition of the late sodium current. Hence, both the substrate (increased dispersion of repolarisation) and the trigger (EADs) for functional reentry and TdP are influenced by AZD7009 as compared to a conventional class III drug.

Since inhibition of the late sodium current by AZD7009 was frequency dependent, with a greater inhibition at higher frequency, it is reasonable to assume that the inhibition will increase when the heart rate is increased. Thus, one might hypothesize that, if increased APD leads to excessive repolarisation prolongation, EADs and triggered activity, the potentiated inhibition of the late sodium current at higher heart rates would tend to abbreviate the APD and suppress the proarrhythmia. In fact, as described in paper III and in the paper by Wu et al. (Wu et al., 2005), AZD7009 suppressed EADs and TdP induced by selective inhibition of IK_r.

Because of the discrepancies in the amount of inhibition of ICa_L by AZD7009, the contribution of ICa_L blockade to the low proarrhythmic potential of AZD7009 is uncertain. In the case of the antiarrhythmic agent H 345/52, inhibition of ICa_L in isolated rabbit cardiomyocytes was dependent upon frequency and membrane potential, with a large inhibition at higher frequencies and depolarised potentials (Amos et al., 2001). If such a frequency- and state-dependence of the block is also present in the case of AZD7009, the contribution of the inhibition of ICa_L may be substantial. However, until the potency-, frequency- and state-dependence of the block of human ICa_L have been more clearly defined, the impact of inhibition of ICa_L on the mechanism of action of AZD7009 will remain unclear.

The ability of sodium or calcium current inhibition to counteract class III-induced APD prolongation and EADs has been known for some time (Abrahamsson et al., 1996; Carlsson et al., 1993b; January et al., 1989).

However, some of the antiarrhythmic drugs on the market that are known to induce TdP in the clinic actually inhibit both repolarising and depolarising currents, e.g. quinidine which inhibits the cardiac sodium current, L-type calcium current and repolarising potassium currents (IK_r, I_{to}, IK_{ur}) (Grace et al., 1998; Selzer et al., 1964).

In the case of quinidine, excessive prolongation of the APD and induction of EADs are seen at low concentrations of the drug and at slow heart rates and is thought to be explained by the reverse frequency dependence of the compound leading to an increased block of IK_r and decreased block of INa at low frequencies (Roden et al., 1985). Reverse frequency dependence is absent or very small in the case of AZD7009. In dog atrial tissue, prolongation of the APD_{90} by AZD7009 was not influenced by changes in the stimulation frequency, indicating the absence of reverse frequency dependence (Carlsson et al., 2006). Similar to the prolongation of the APD, the effect of AZD7009 on AERP and VERP in the dog *in vivo* was not dependent on the stimulation frequency (Carlsson et al., 2006). In the canine left ventricular wedge preparation, however, there was a small but significant increase in transmural dispersion of repolarisation at the longest basic cycle length (2000ms), but not at shorter basic cycle lengths (500 and 1000 ms), indicating a small reverse use dependence in the ventricle. However, the increase was considerably smaller than that seen for dofetilide (Wu et al., 2005).

The antianginal agent ranolazine is an example of a drug that inhibits IK_r, the late sodium current and, at lower potency, the late calcium current and possesses a low proarrhythmic potential (Antzelevitch et al., 2004). The ranolazine-induced inhibition of the late sodium current is dependent on the stimulation frequency, with a more pronounced inhibition at increased frequency. Ranolazine produced a rate-independent decrease of the transmural dispersion of repolarisation, and EADs could not be induced in the presence of ranolazine alone or in combination with sotalol (Antzelevitch et al., 2004).

It is important to note that the protective effect of inhibition of inward currents (e.g. the late sodium current) must not be separated from the inhibition of outward currents (e.g. IK_r) with too great a difference in effective concentrations. The inhibition of the inward current would theoretically be less protective against proarrhythmia if there is a large concentration difference in the inhibition of inward and outward currents (Yan et al., 2002). In the case of AZD7009, concentration differences are seen in the IC_{50} values for the inhibition of hERG and Nav1.5 (papers I and

III). The effects of AZD7009 on the sodium current were recently studied in dog atrial tissue using Vmax as an index of the sodium current. It was shown that Vmax was already significantly suppressed by AZD7009 at 0.4 μM, a concentration that did not influence APD (Carlsson et al., 2006). Hence, the potency of the sodium current inhibition has likely been underestimated in the voltage-clamp recordings; a possible explanation is that the voltage-clamp recordings were done at room temperature and the measurements of Vmax at 37°C.

In addition to the inhibition of the late sodium current by AZD7009, the absence of a prominent inhibition of KvLQT1/minK (IK_s) and the presence of a prepulse potentiation of the hERG current (IK_r) (paper I) would leave a repolarisation reserve that may maintain adequate repolarisation capacity during phase 3. Volders and coworkers noted that the importance of IK_s for the late repolarisation in dog ventricle is greater during inhibition of IK_r (Volders et al., 2003). Prepulse potentiation of hERG has been described for other antiarrhythmic agents, e.g. azimilide (Jiang et al., 1999) and almokalant (Carmeliet, 1993). However, almokalant, which is a selective IK_r-inhibiting compound, has the potential to induce TdP in the methoxamine-sensitised rabbit model and in man (Carlsson et al., 1993a; Darpö et al., 1996). Hence, the prepulse potentiation of hERG can not by itself explain the low proarrhythmic potential of AZD7009 but may contribute when combined with other protective properties.

CONCLUSIONS

- AZD7009 blocked human ion channels expressed in CHO cells. The hERG channel was most potently blocked, while the Nav1.5, the Kv4.3/KChIP2.2 and the Kv1.5 channels were blocked with an intermediate and the Kir3.1/Kir3.4 and KvLQT1/minK with a low potency.

- AZD7009 inhibited the late sodium current in rabbit atrial and ventricular myocytes and with lower potency the L-type calcium current in rabbit ventricular myocytes and H9c2 cells.

- AZD7009 prolonged the APD in rabbit atrial and ventricular tissue and in Purkinje fibre.

- AZD7009 counteracted excessive APD prolongation and EADs induced by selective IK_r blockade in Purkinje fibre, whereas the APD in ventricular tissue was not changed and the APD in atrial tissue was further prolonged.

- A synergistic inhibition of IK_r, I_{to} and IK_{ur} and a larger impact on the inhibition of the late sodium current in the ventricle may explain the predominant action of AZD7009 on atrial electrophysiological parameters.

- Inhibition of repolarising potassium currents (IK_r, I_{to} and IK_{ur}) and the cardiac sodium current, leading to a prolonged APD and an increased ERP, may explain the high antiarrhythmic efficacy of AZD7009 for termination of AF.

- The inhibition of the late sodium current, the prepulse potentiation of hERG at near threshold potentials and the absence of IK_s inhibition at physiologically relevant concentrations may explain the low proarrhythmic potential of AZD7009.

FUTURE DIRECTIONS

The knowledge of the ion channel blocking profile of AZD7009 obtained so far has provided a possible explanation of the mechanism behind the atrial selectivity, efficacy and low proarrhythmic potential of the drug. However, some uncertainties in the ion channel blocking profile of AZD7009 are still present. For example, the effect of AZD7009 on ICa_L must be examined in more detail, specifically the frequency- and state-dependence of block, and ICa_L must be studied either in human cardiomyocytes or in a cell line expressing human ICa_L. In addition to ICa_L, it would also be valuable to study the effects of AZD7009 on ICa_T, I_f and ion transporters, e.g. the sodium-calcium exchanger.

A drawback in the ion channel studies presented here is that they have all been carried out at room temperature. Studies of ion current inhibition by AZD7009 at physiologic temperature, especially for the sodium current, would help in the interpretation of ion channel blocking data.

Mutational studies of ion channels, e.g. hERG, to be able to pinpoint the binding site of AZD7009 and to compare the binding site with other compounds would also add important information.

Despite the excellent efficacy of AZD7009 in terminating AF in patients (Crijns et al., 2006), its clinical development was recently stopped on the grounds of unforeseen noncardiovascular side effects. However, there is a great need for an effective and safe antiarrhythmic drug for restoration and maintenance of sinus rhythm and it will remain. Although AZD7009 will never reach the market, the concept of a multi-ion channel block for effective and safe antiarrhythmic treatment has been proven, and other compounds with a similar mechanism of action will follow in its footsteps.

POPULÄRVETENSKAPLIG SAMMANFATTNING

Ju äldre en människa blir desto större är risken för att utveckla förmaksflimmer. Med en åldrande befolkning blir förmaksflimmer allt vanligare. I EU-länderna är 4,5 miljoner personer drabbade. Sjukdomen leder till nedsatt hjärtfunktion och ökad dödlighet. Ett idealiskt läkemedel mot förmaksflimmer borde påverka hjärtats förmak utan att ge några effekter på dess kammare. Dagens läkemedel mot förmaksflimmer har stor påverkan på hjärtats kammare och kan där vara proarytmiska vilket betyder att de kan ge upphov till ojämn rytm – arytmi – vilket är en svår biverkning som kan leda till kammarflimmer och plötslig död.

AZD7009 är en ny substans mot förmaksflimmer som i studier på både djur och människa har visat sig ha större effekt på hjärtats förmak än den har på dess kammare. AZD7009 återför förmaksflimmer till hjärtats normala rytm – sinusrytm – utan att ge upphov till proarytmi. Syftet med denna avhandling är att förklara vad som gör att AZD7009 har god effekt mot förmaksflimmer utan att ge upphov till proarytmi.

En aktionspotential beskriver summan av den elektriska aktiviteten i hjärtat när det slår. Varje enskild cell har en aktionspotential per kontraktion (slag). Några av de begrepp som används för att beskriva aktionspotentialen är depolarisering, som beskriver den snabba uppgången i början på aktionspotentialen, platå, som är perioden innan återgång till viloläge startar, repolarisering, som är återgången till viloläge samt refraktärperiod, som är tiden efter en aktionspotential innan nästa aktionspotential kan utlösas.

Aktionspotentialen styrs av strömmar av joner som leds via proteiner i hjärtmuskelcellernas cellmembran. Dessa proteiner kallas jonkanaler. Jonkanaler kan leda olika typer av joner; vanligast är kalium- (K^+), natrium- (Na^+) och kalcium- (Ca^{2+}) joner. Jonkanalerna namnges oftast utifrån vilken jon som passerar lättast genom kanalen; således finns det K^+-kanaler, Na^+-kanaler och Ca^{2+}-kanaler. Exempel på olika K^+-kanaler i hjärtat är hERG, Kv4.3/KChIP2.2, Kv1.5, Kir3.1/Kir3.4 och KvLQT1/minK. Varje jonkanal ger upphov till en jonström till exempel ger hERG upphov till IK_r, Kv4.3/KChIP2.2 till I_{to} och Kv1.5 till IK_{ur}. Natriumkanalen i hjärtat benämns Nav1.5 och ger upphov till jonströmmen INa som har en tidig och en sen komponent. Den tidiga komponenten är viktig för den snabba depolariseringen av aktionspotentialen medan den sena komponenten bidrar

till att förlänga platån och fördröja repolariseringen. Den viktigaste Ca^{2+}-kanalen i hjärtat ger upphov till en L-typ Ca^{2+}-ström som är viktig dels för att koppla samman aktionspotentialen med hjärtats kontraktion dels för att förlänga aktionspotentialens platå och fördröja dess repolarisering.

Effekten av AZD7009 på jonströmmar och jonkanaler studerades med en teknik som kallas voltage-clamp. Voltage-clamp innebär att en elektrod ansluts till en enskild cell varvid jonströmmarna över cellens cellmembran kan mätas. Studierna gjordes på dels transfekterade däggdjursceller, vilket betyder att en human gen sätts in i cellerna och förmår dem att producera den mänskliga varianten av en jonkanal, dels på celler som hämtats (akutisolerats) från hjärtats förmak och kammare hos kanin. Försöken har fastställt vilken effekt AZD7009 har på olika jonkanaler; bland annat har ett antal IC_{50}-värden fastställts. De anger vilken koncentration som krävs av substansen för att hämma jonströmmarna till 50 procent. IC står för ”inhibitory concentration”. AZD7009 hämmade jonströmmarna genom de humana jonkanalerna i transfekterade däggdjursceller med följande IC_{50}-värden: hERG 0.6 µM, Nav1.5 8 µM, Kv4.3/KChIP2.2 24 µM, Kv1.5 27 µM, Kir3.1/Kir3.4 166 µM och KvLQT1/minK 193 µM. hERG hämmades alltså med högst potens och KvLQT1/minK med lägst potens.

I akutisolerade hjärtmuskelceller från kaninförmak och -kammare hämmades den sena Na^{+}-strömmen av AZD7009 med motsvarande potens som Nav1.5 i transfekterade däggdjursceller. L-typ Ca^{2+}-ström i akutisolerade hjärtmuskelceller från kaninkammare hämmades med ett IC_{50}-värde på 90 µM.

I vävnadsbitar från kanin mättes aktionspotentialens längd (förkortas APD efter det engelska ”action potential duration”) i förmak, kammare och Purkinjefibrer. Det senare är en del av det så kallade retledningssystemet som sprider den elektriska aktiviteten över kamrarna. Vissa av mätningarna gjordes i närvaro av en substans, E-4031, som har förmåga att selektivt hämma en specifik jonström IK_r. Eftersom IK_r bidrar till repolarisering av aktionspotentialen kan således längden på den elektriska aktiviteten – APD – förlängas med hjälp av E-4031. Mätningarna gjordes dels i närvaro av E-4031 ensamt, dels i kombination med AZD7009 eller lidokain. Lidokain är en substans som selektivt hämmar Na^{+}-strömmen. Det visade sig att den förlängning av APD som E-4031 ger upphov till motverkades av AZD7009 och lidokain i Purkinjefibrer men inte i hjärtats kammarmuskelceller. I förmaket förlängde AZD7009 APD ytterligare men lidokain hade ingen sådan effekt.

En alltför kraftig förlängning av APD i kammaren kan leda till att sekundära depolariseringar uppkommer under aktionspotentialens platå eller repolarisering. Dessa sekundära depolariseringar kallas EAD, efter det engelska early afterdepolarisation. EAD kan leda till proarytmi. I försöken gav E-4031 en kraftig förlängning av APD och utlöste EAD i Purkinjefibrer. Dessa EAD kunde motverkas av AZD7009 och lidokain.

Sammanfattningsvis, AZD7009 hämmar flera av hjärtats jonströmmar främst IK_r, INa, I_{to} och IK_{ur} vilket leder till en förlängning av APD och hjärtats refraktärperiod vilket motverkar förmaksflimmer. Orsaken till att effekten är större på hjärtats förmak än kammare är troligen en synergistisk effekt av hämning av IK_r, I_{to} och den förmaksselektiva IK_{ur} vilket ger en ökad förlängning av APD i förmaken än i kamrarna. Den låga risken för proarytmiska effekter kan förklaras med att hämning av Na^+-strömmens sena komponent motverkar en alltför kraftig förlängning av APD och utlösandet av EAD i Purkinjefibrer och andra känsliga celler i hjärtats kammare.

ACKNOWELEDGEMENTS

I would like to thank all my friends and colleagues who have supported and helped me during my years of research, especially:

Ingemar Jacobson, my supervisor, who has guided me into the world of electrophysiology and ion channels and always has had the time for questions.

Holger Wigström, my university supervisor, for letting me be part of the Department of Medical Biophysics and guiding me through the university administration.

Leif Carlsson and Göran Duker for sharing your knowlegde, carefully reading and commenting the manuscripts and the summary and for your continuous support and encouragement.

Birgit Andersson for excellent action potential recordings.

Anita Carlsson, Elin Forsström, Gunilla Linhardt, Lena Löfberg, May Sjölander and everyone else in the arrhythmia group for making HF3 such a great place to work.

Per Ove Sjöquist and Peter Thorén for giving me the opportunity to combine my PhD studies with my work at AstraZeneca R&D Mölndal.

Nils-Olov Hermansson for support with the Kir3.1/Kir3.4 cells.

The technical support group for excellent service, especially Lars-Eric Marberg for providing me with technical equipment for the voltage-clamp lab.

'Choklad klubben' for lunch breaks worth waiting for and for discussions about all and nothing.

Åke Wessman for making the Swedish summary readable.

Janet Vesterlund for kindly revising the English in this summary.

Most of all I would like to thank my family.

REFERENCES

1989. Preliminary report: effect of encainide and flecainide on mortality in a randomized trial of arrhythmia suppression after myocardial infarction. The Cardiac Arrhythmia Suppression Trial (CAST) Investigators. N Engl J Med 321, 406-412.

Abbott, G.W., Sesti, F., Splawski, I., Buck, M.E., Lehmann, M.H., Timothy, K.W., Keating, M.T., Goldstein, S.A.N., 1999. MiRP1 forms IKr potassium channels with HERG and is associated with cardiac arrhythmia. Cell 97, 175-187.

Abrahamsson, C., Carlsson, L., Duker, G., 1996. Lidocaine and nisoldipine attenuate almokalant-induced dispersion of repolarisation and early after depolarisations in vitro. J Cardiovasc Electrophysiol 7, 1074-1081.

Amos, G.J., Abrahamsson, C., Duker, G., Hondeghem, L., Palmer, M., Carlsson, L., 2001. Potassium and calcium current blocking properties of the novel antiarrhythmic agent H 345/52: implications for proarrhythmic potential. Cardiovasc Res 49, 351-360.

Amos, G.J., Wettwer, E., Metzger, F., Li, Q., Himmel, H.M., Ravens, U., 1996. Differences between outward currents of human atrial and subepicardial ventricular myocytes. J Physiol 491, 31-50.

An, W.F., Bowlby, M.R., Betty, M., Cao, J., Ling, H.-P., Mendoza, G., Hinson, J.W., Mattsson, K.I., Strassle, B.W., Trimmer, J.S., Rhodes, K.J., 2000. Modulation of A-type potassium channels by a family of calcium sensors. Nature 403, 553-556.

Anantharam, A., Abbott, G.W., 2005. Does hERG coassemble with a beta subunit? Evidence for roles of MinK and MiRP1. Novartis Foundation Symposium 266, 100-117.

Antzelevitch, C., Belardinelli, L., Zygmunt, A.C., Burashnikov, A., Di Diego, J., Fish, J.M., Cordeiro, J.M., Thomas, G., 2004. Electrophysiological effects of ranolazine, a novel antianginal agent with antiarrhythmic properties. Circulation 110, 904-910.

Antzelevitch, C., Oliva, A., 2006. Amplification of spatial dispersion of repolarisation underlies sudden cardiac death associated with catecholaminergic polymorphic VT, long QT, short QT and Brugada syndromes. J Int Med 259, 48-58.

Authors/Task Force Members, Fuster, V., Ryden, L.E., Cannom, D.S., Crijns, H.J., Curtis, A.B., Ellenbogen, K.A., Halperin, J.L., Le Heuzey, J.-Y., Kay, G.N., Lowe, J.E., Olsson, S.B., Prystowsky, E.N., Tamargo, J.L., Wann, S., ESC Committee for Practice Guidelines, Priori, S.G., Blanc, J.-J., Budaj, A., Camm, A.J., Dean, V., Deckers, J.W., Despres, C., Dickstein, K., Lekakis, J., McGregor, K., Metra, M., Morais, J., Osterspey, A., Zamorano, J.L., ACC/AHA

(Practice Guidelines) Task Force Members, Smith, S.C., Jr, Jacobs, A.K., Adams, C.D., Anderson, J.L., Antman, E.M., Hunt, S.A., Nishimura, R., Ornato, J.P., Page, R.L., Riegel, B., 2006. ACC/AHA/ESC 2006 guidelines for the management of patients with atrial fibrillation. Eur Heart J 27, 1979-2030.

Barhanin, J., Lesage, F., Guillemare, E., Fink, M., Lazdunski, M., Romey, G., 1996. KvLQT1 and IsK (minK) proteins associate to form the IKs cardiac potassium current. Nature 384, 78-80.

Baruscotti, M., Bucchi, A., DiFrancesco, D., 2005. Physiology and pharmacology of the cardiac pacemaker ("funny") current. Pharmacol Ther 107, 59-79.

Belardinelli, L., Antzelevitch, C., Vos, M.A., 2003. Assessing predictors of drug-induced torsade de pointes. Trends Pharmacol Sci 24, 619-625.

Belardinelli, L., Shryock, J.C., Fraser, H., 2006. Inhibition of the late sodium current as a potential cardioprotective principle: effects of the late sodium current inhibitor ranolazine. Heart 92, 6-14.

Bett, G., Noble, D., Noble, S., Earm, Y., Ho, W.K., So, I.S., 1992. Na-Ca exchange current during the cardiac action potential. Adv Exp Med Biol 311, 453-454.

Blaauw, Y., Goegelein, H., Duytschaever, M., Tieleman, R.G., Schotten, U., Allessie, M.A., 2003. Synergistic class III action of blockade of IKur/Ito (AVE0118) and IKr (dofetilide/ibutilide) in electrically remodeled atria of the goat. Circulation 108, IV-84.

Bosch, R.F., Zeng, X., Grammer, J.B., Popovic, K., Mewis, C., Kuhlkamp, V., 1999. Ionic mechanisms of electrical remodeling in human atrial fibrillation. Cardiovasc Res 44, 121-131.

Boutjdir, M., Le Heuzey, J.Y., Lavergne, T., Chavaud, S., Guize, L., 1986. Inhomogeneity of cellular refractoriness in human atrium: factor of arrhythmia? PACE 9, 1095-1100.

Brendel, J., Wirth, K., Goegelein, H., Allessie, M.A., Blaauw, Y., 2004. Phenylcarboxyl acid amindes and IKr channel inhibitors combination and the use thereof for treating atrial arrhythmia. Patent application WO 2004/082716 A082711.

Brundel, B.J.J.M., Van Gelder, I.C., Henning, R.H., Tuinenburg, A.E., Deelman, L.E., Tieleman, R.G., Grandjean, J.G., Van Gilst, W.H., Crijns, H.J.G.M., 1999. Gene expression of proteins influencing the calcium homeostasis in patients with persistent and paroxysmal atrial fibrillation. Cardiovasc Res 42, 443-454.

Brundel, B.J.J.M., Van Gelder, I.C., Henning, R.H., Tuinenburg, A.E., Wietses, M., Grandjean, J.G., Wilde, A.A.M., Van Gilst, W.H., Crijns, H.J., 2001. Alterations in potassium channel gene expression in atria of patients with persistent and paroxysmal atrial fibrillation:

differential regulation of protein and mRNA levels for K+ channels. J Am Coll Cardiol 37, 926-932.

Bähring, R., Dannenberg, J., Peters, H.C., Leicher, T., Pongs, O., Isbrandt, D., 2001. Conserved Kv4 N-terminal domain critical for effects of Kv channel-interacting protein 2.2 on channel expression and gating. J Biol Chem 276, 23888-23894.

Camm, J., 2006. Medical management of atrial fibrillation: state of the art. J Cardiovasc Electrophysiol 17, S2-S6.

Campbell, T.J., 1989, Subclassification of class I antiarrhythmic drugs, in: *Antiarrhythmic Drugs*, ed. Vaughan-Williams, E.M. (Springer-Verlag, 135-155.

Carlsson, L., 2006. In vitro and in vivo models for testing arrhythmogenesis in drugs. J Int Med 259, 70-80.

Carlsson, L., Abrahamsson, C., Andersson, B., Duker, G., Schiller-Linhardt, G., 1993a. Proarrhythmic effects of the class III agent almokalant: importance of infusion rate, QT dispersion, and early afterdepolarisations. Cardiovasc Res 27, 2186-2193.

Carlsson, L., Almgren, O., Duker, G., 1990. QTU-prolongation and torsades de poites induced by putative class III antiarrhythmic agents in the rabbit: etiology and interventions. J Cardiovasc Pharmacol 16, 276-285.

Carlsson, L., Chartier, D., Nattel, S., 2006. Characterization of the in vivo and in vitro electrophysiological effects of the novel antiarrhythmic agent AZD7009 in atrial and ventricular tissue of the dog. J Cardiovasc Pharmacol 47, 123-132.

Carlsson, L., Drews, L., Duker, G., Schiller-Linhardt, G., 1993b. Attenuation of proarrhythmias related to delayed repolarization by low- dose lidocaine in the anesthetized rabbit. J Pharmacol Exp Ther 267, 1076-1080.

Carlsson, L., Duker, G., Linhardt, G., 2004. AZD7009-A new atrial antifibrillatory compound that markedly delays atrial refractoriness and possesses low proarrhythmic activity in the anaesthetised rabbit. Eur Heart J 6, P2939.

Carmeliet, E., 1992. Voltage- and time-dependent block of the delayed K+ current in cardiac myocytes by dofetilide. J Pharmacol Exp Ther 262, 809-817.

Carmeliet, E., 1993. Use-dependent block and use-dependent unblock of the delayed rectifier K+ current by almokalant in rabbit ventricular myocytes. Circ Res 73, 857-868.

Carmeliet, E., Mubagwa, K., 1998. Antiarrhythmic drugs and cardiac ion channels: mechanism of action. Prog Biophys Mol Biol 70, 1-72.

Carmeliet, E., Vereecke, J., 2002a, Genesis of the ECG wave, in: *Cardiac Cellular Electrophysiology* (Kluwer Academic Publishers, Dordrecht/Boston/London) 239-243.

Carmeliet, E., Vereecke, J., 2002b, Ion currents in cardiac plasma membranes, in: *Cardiac Cellular Electrophysiology* (Kluwer Academic Publishers, Dorderecht/Boston/London) 95-143.

Cerbai, E., Mugelli, A., 2006. If in non-pacemaker cells: role and pharmacological implications. Pharmacol Res 53, 416-423.

Cheng, J., 2006. Evidences of the gender-related differences in cardiac repolarization and the underlying mechanisms in different animal species and human. Fund Clin Pharmacol 20, 1-8.

Clancy, C.E., Tateyama, M., Liu, H., Wehrens, X.H.T., Kass, R.S., 2003. Non-equilibrium gating in cardiac Na+ channels: an original mechanism of arrhythmia. Circulation 107, 2233-2237.

Clay, J.R., 2000. Determining K+ channel activation curves from K+ channel currents. Eur Biophys J 29, 555-557.

Cosio, F.G., Delpon, E., 2002. New antiarrhythmic drugs for atrial flutter and atrial fibrillation: a conceptual breakthrough at last? Circulation 105, 276-278.

Courtemanche, M., Ramirez, R.J., Nattel, S., 1999. Ionic targets for drug therapy and atrial fibrillation-induced electrical remodeling: insights from a mathematical model. Cardiovasc Res 42, 477-489.

Cribbs, L.L., Lee, J.-H., Yang, J., Satin, J., Zhang, Y., Daud, A., Barclay, J., Williamson, M.P., Fox, M., Rees, M., Perez-Reyes, E., 1998. Cloning and characterization of alpha1H from human heart, a member of the T-type Ca2+ channel gene family. Circ Res 83, 103-109.

Crijns, H.J., Van Gelder, I.C., Walfridsson, H., Kulakowski, P., Ronaszeki, A., Dedek, V., Malm, A., Almgren, O., 2006. Safe and effective conversion of persistent atrial fibrillation to sinus rhythm by intravenous AZD7009. Heart Rhythm 3, 1321-1331.

Crijns, H.J.G.M., 2005. Rate versus rhythm control in patients with atrial fibrillation. What the trials really say. Drugs 65, 1651-1667.

D'Ambrosio, R., 2002, Perforated patch-clamp technique, in: *Patch-Clamp Analysis - Advanced Techniques*, eds. Walz, W., Boulton, A.A., Baker, G.B. (Humana press, Totowa, New Jersey) 195-216.

Darpö, B., Allared, M., Edvardsson, N., 1996. Torsades de pointes induced by transesophageal atrial stimulation after administration of almokalant. Int J Cardiol 53, 311-313.

Decher, N., Uyguner, O., Scherer, C.R., Karaman, B., Yüksel-Apak, M., Busch, A.E., Steinmeyer, K., Wollnik, B., 2001. hKChIP2 is a functional modifier of hKv4.3 potassium channels: cloning and

expression of a short hKChIP2 splice variant. Cardiovasc Res 52, 255-264.
Desertenne, F., 1966. La tachycardie ventriculaire a deux foyers opposes varibles. Arch Mal Coeur 59, 263-272.
Dhamoon, A.S., Jalife, J., 2005. The inward rectifier current (IK1) controls cardiac excitability and is involved in arrhythmogenesis. Heart Rhythm 2, 316-324.
DiFrancesco, D., 2006. Funny channels in the control of cardiac rhythm and mode of action of selective blockers. Pharmacol Res 53, 399-406.
Dixon, J.E., Shi, W., Wang, H.-S., McDonald, C., Yu, H., Wymore, R.S., Cohen, I.S., McKinnon, D., 1996. Role of the Kv4.3 K+ channel in ventricular muscle: a molecular correlate for the transient outward current. Circ Res 79, 659-668.
Dobrev, D., Friedrich, A., Voigt, N., Jost, N., Wettwer, E., Christ, T., Knaut, M., Ravens, U., 2005. The G protein-gated potassium current IK,ACh is constitutively active in patients with chronic atrial fibrillation. Circulation 112, 3697-3706.
Dobrev, D., Ravens, U., 2003. Remodeling of cardiomyocyte ion channels in human atrial fibrillation. Basic Res Cardiol 98, 137-148.
Doyle, D.A., Cabral, J.M., Pfuetzner, R.A., Kuo, A., Gulbis, J.M., Cohen, S.L., Chait, B.T., MacKinnon, R., 1998. The structure of the potassium channel: molecular basis of K+ conduction and selectivity. Science 280, 69-77.
Drouin, E., Charpentier, F., Gauthier, C., Laurent, K., Le Marec, H., 1995. Electrophysiologic characteristics of cells spanning the left ventricular wall of human heart: evidence for presence of M Cells. J Am Coll Cardiol 26, 185-192.
Duker, G., Andersson, B., Jacobson, I., Linhardt, G., Nordstrom, A., Carlsson, L., 2005. Antiarrhythmic efficacy and electrophysiological characteristics of AZD7009 in dogs with pacing-induced atrial fibrillation and remodelling. Eur Heart J 26, 507.
Duker, G., Björkman, J.-A., Linhardt, G., Carlsson, L., 2004. AZD7009- A new atrial antifibrillatory compound that markedly delays atrial refractoriness in the anaesthetised dog. Heart Rhythm 1, S159.
Edvardsson, N., Walfridsson, H., Aass, H., Rossvoll, O., 2005. Predominant effects on atrial versus ventricular refractoriness in man by the novel antiarrhythmic agent AZD7009. Eur Heart J 26, 506.
Fedida, D., Eldstrom, J., Hesketh, J.C., Lamorgese, M., Castel, L., Steele, D.F., Van Wagoner, D.R., 2003. Kv1.5 is an important component of repolarizing K+ current in canine atrial myocytes. Circ Res 93, 744-751.

Fedida, D., Orth, P.M.R., Hesketh, J.C., Ezrin, A.M., 2006. The role of late INa and antiarrhythmic drugs in EAD formation and termination in Purkinje fibers. J Cardiovasc Electrophysiol 17, S71-78.

Feng, J., Wible, B., Li, G.-R., Wang, Z., Nattel, S., 1997. Antisense oligodeoxynucleotides directed against Kv1.5 mRNA specifically inhibit ultrarapid delayed rectifier K+ current in cultured adult human atrial myocytes. Circ Res 80, 572-579.

Franqueza, L., Valenzuela, C., Delpon, E., Longobardo, M., Caballero, R., Tamargo, J., 1998. Effects of propafenone and 5-hydroxy-propafenone on hKv1.5 channels. Br J Pharmacol 125, 969-978.

Gaborit, N., Steenman, M., Lamirault, G., Le Meur, N., Le Bouter, S., Lande, G., Leger, J., Charpentier, F., Christ, T., Dobrev, D., Escande, D., Nattel, S., Demolombe, S., 2005. Human atrial ion channel and transporter subunit gene-expression remodeling associated with valvular heart disease and atrial fibrillation. Circulation 112, 471-481.

Gabriel, S.E., Price, E.M., Boucher, R.C., Stutts, M.J., 1992. Small linear chloride channels are endogenous to nonepithelial cells. Am J Physiol Cell Physiol 263, C708-713.

Gaspo, R., Bosch, R.F., Bou-Abboud, E., Nattel, S., 1997. Tachycardia-induced changes in Na+ current in a chronic dog model of atrial fibrillation. Circ Res 81, 1045-1052.

Gellens, M., George, A., Jr, Chen, L., Chahine, M., Horn, R., Barchi, R., Kallen, R., 1992. Primary structure and functional expression of the human cardiac tetrodotoxin-insensitive voltage-dependent sodium channel. Proc Natl Acad Sci U S A 89, 554-558.

Goldstein, R.N., Khrestian, C., Carlsson, L., Waldo, A.L., 2004. AZD7009: A new antiarrhythmic drug with predominant effects on the atria effectively terminates and prevents reinduction of atrial fibrillation and flutter in the sterile pericarditis model. J Cardiovasc Electrophysiol 15, 1444-1450.

Grace, A.A., Camm, A.J., 1998. Quinidine. N Engl J Med 338, 35-45.

Gögelein, H., Brendel, J., Steinmeyer, K., Strubing, C., Picard, N., Rampe, D., Kopp, K., E, B.A., Bleich, M., 2004. Effects of the atrial antiarrhythmic drug AVE0118 on cardiac ion channels. Naunyn-Schmiedbergs Arch. Pharmacol. 370, 183-192.

Hamill, O.P., Marty, A., Neher, E., Sakmann, B., Sigworth, F.J., 1981. Improved patch-clamp techniques for high-resolution current recording from cells and cell-free membrane patches. Pflugers Arch 391, 85-100.

Hatano, N., Ohya, S., Muraki, K., Giles, W., Imaizumi, Y., 2003. Dihydropyridine Ca2+ channel antagonists and agonists block Kv4.2,

Kv4.3 and Kv1.4 K+ channels expressed in HEK293 cells. Br J Pharmacol 139, 533-544.

Herfst, L.J., Rook, M.B., Jongsma, H.J., 2004. Trafficking and functional expression of cardiac Na+ channels. J Mol Cell Cardiol 36, 185-193.

Hescheler, J., Meyer, R., Plant, S., Krautwurst, D., Rosenthal, W., Schultz, G., 1991. Morphological, biochemical, and electrophysiological characterization of a clonal cell (H9c2) line from rat heart. Circ Res 69, 1476-1486.

Hohnloser, S.H., Singh, B.N., 1995. Proarrhythmia with class III antiarrhythmic drugs: defenition , electrophysiologic mechanisms, incidence, predisposing factors, and clinical implications. J Cardiovasc Electrophysiol 6, 920-936.

January, C.T., Riddle, J.M., 1989. Early afterdepolarizations: mechanism of induction and block. A role for L-type Ca2+ current. Circ Res 64, 977-990.

Jiang, M., Dun, W., Fan, J.-S., Tseng, G.-N., 1999. Use-dependent agonist effect of azimilide on the HERG channel. J Pharmacol Exp Ther 291, 1324-1336.

Jiang, Y., Ruta, V., Chen, J., Lee, A., MacKinnon, R., 2003. The principle of gating charge movement in a voltage-dependent K+ channel. Nature 423, 42-48.

Johns, J.A., Anno, T., Bennett, P.B., Snyders, D.J., Hondeghem, L., 1989. Temperature and voltage dependence of sodium channel blocking and unblocking by O-demethyl encainide in isolated guinea pig myocytes. J Cardiovasc Pharmacol 13, 826-835.

Jost, N., Virag, L., Bitay, M., Takacs, J., Lengyel, C., Biliczki, P., Nagy, Z., Bogats, G., Lathrop, D.A., Papp, J.G., Varro, A., 2005. Restricting excessive cardiac action potential and QT prolongation: a vital role for IKs in human ventricular muscle. Circulation 112, 1392-1399.

Kane, G.C., Liu, X.-K., Yamada, S., Olson, T.M., Terzic, A., 2005. Cardiac KATP channels in health and disease. J Mol Cell Cardiol 38, 937-943.

Kimes, B.W., Brandt, B.L., 1976. Properties of a clonal muscle cell line from rat heart. Exp Cell Res 98, 367-381.

Kong, W., Po, S., Yamagishi, T., Ashen, M.D., Stetten, G., Tomaselli, G.F., 1998. Isolation and characterization of the human gene encoding Ito: further diversity by alternative mRNA splicing. Am J Physiol Heart Circ Physiol 275, H1963-1970.

Krapivinsky, G., Gordon, E.A., Wickman, K., Velimirovic, B., Krapivinsky, L., Clapham, D.E., 1995. The G-protein-gated atrial K+ channel IKAch is a heteromultimer of two inwardly rectifying K+-channel proteins. Nature 374, 135-141.

Kubo, Y., Baldwin, T.J., Jan, Y.N., Jan, L.Y., 1993. Primary structure and functional expression of a mouse inward rectifier potassium channel. Nature 362, 127-133.

Li, D., Fareh, S., Leung, T.K., Nattel, S., 1999. Promotion of atrial fibrillation by heart failure in dogs : atrial remodeling of a different sort. Circulation 100, 87-95.

Li, G.-R., Feng, J., Yue, L., Carrier, M., 1998. Transmural heterogeneity of action potentials and Ito1 in myocytes isolated from the human right ventricle. Am J Physiol Heart Circ Physiol 275, H369-377.

Li, G.-R., Feng, J., Yue, L., Carrier, M., Nattel, S., 1996. Evidence for two components of delayed rectifier K+ current in human ventricular myocytes. Circ Res 78, 689-696.

Li, Y., Um, S.Y., McDonald, T.V., 2006. Voltage-gated potassium channels: regulation by accessory subunits. Neuroscientist 12, 199-210.

Liu, D.-W., Antzelevitch, C., 1995. Characteristics of the delayed rectifier current (IKr and IKs) in canine ventricular epicardial, midmyocardial, and endocardial myocytes : a weaker IKs contributes to the longer action potential of the M cell. Circ Res 76, 351-365.

Liu, H., Atkins, J., Kass, R.S., 2003. Common molecular determinants of flecainide and lidocaine block of heart Na+ channels: evidence from experiments with neutral and quaternary flecainide analogues. J Gen Physiol 121, 199-214.

Liu, H., Tateyama, M., Clancy, C.E., Abriel, H., Kass, R.S., 2002. Channel openings are necessary but not sufficient for use-dependent block of cardiac Na+ channels by flecainide: evidence from the analysis of disease-linked mutations. J Gen Physiol 120, 39-51.

Long, S.B., Campbell, E.B., MacKinnon, R., 2005. Crystal structure of a mammalian voltage-dependent shaker family K+ channel. Science 309, 897-903.

Lopatin, A.N., Nichols, C.G., 2001. Inward rectifiers in the heart: an update on IK1. J Mol Cell Cardiol 33, 625-638.

Lorenz, E., Terzic, A., 1999. Physical association between recombinant cardiac ATP-sensitive K+channel subunits Kir6.2 and SUR2A. J Mol Cell Cardiol 31, 425-434.

Löfberg, L., Jacobson, I., Carlsson, L., 2006. Electrophysiological and antiarrhythmic effects of the novel antiarrhythmic agent AZD7009: a comparision with azimilide and AVE0118 in acutely dilated right atrium of the rabbit in vitro. Europace 8, 549-557.

Makary, S.M.Y., Claydon, T.W., Entvetchakul, D., Nichols, C.G., Boyett, M.R., 2005. A difference in inward rectification and polyamine block and permeation between Kir2.1 and Kir3.1/Kir3.4 K+ channels. J Physiol 568, 749-766.

Maltsev, V.A., Sabbah, H.N., Higgins, R.S.D., Silverman, N., Lesch, M., Undrovinas, A.I., 1998. Novel, ultraslow inactivating sodium current in human ventricular cardiomyocytes. Circulation 98, 2545-2552.

Maltsev, V.A., Sabbah, H.N., Undrovinas, A.I., 2001. Late sodium current is a novel target for amiodarone: studies in failing human myocardium. J Mol Cell Cardiol 33, 923-932.

Maltsev, V.A., Undrovinas, A.I., 2006. A multi-modal composition of the late Na+ current in human ventricular cardiomyocytes. Cardiovascular Research 69, 127.

Mangoni, M.E., Couette, B., Marger, L., Bourinet, E., Striessnig, J., Nargeot, J., 2006. Voltage-dependent calcium channels and cardiac pacemaker activity: from ionic currents to genes. Prog Biophys Mol Biol 90, 38-63.

Mazhari, R., Greenstein, J.L., Winslow, R.L., Marban, E., Nuss, H.B., 2001. Molecular interactions between two long-QT syndrome gene products, hERG and KCNE2, rationalized by in vitro and in silico analysis. Circ Res 89, 33-38.

Menard, C., Pupier, S., Mornet, D., Kitzmann, M., Nargeot, J., Lory, P., 1999. Modulation of L-type calcium channel expression during retinoic acid-induced differentiation of H9C2 cardiac cells. J Biol Chem 274, 29063-29070.

Mitcheson, J.S., Chen, J., Sanguinetti, C., 2000. Trapping of a methanesulfonanilide by closure of the HERG potassium channel activation gate. J Gen Physiol 115, 229-239.

Nagatomo, T., January, C.T., Makielski, J.C., 2000. Preferential block of late sodium current in the LQT3 deltaKPQ mutant by the class 1c antiarrhythmic flecainide. Mol Pharmacol 57, 101-107.

Nattel, S., Carlsson, L., 2006. Innovative approaches to anti-arrthytmic drug therapy. Nature Rev Drug Disc 5, 1034-1048.

Nattel, S., Li, D., Yue, L., 2000. Basic mechanisms of atrial fibrillation - very new insights into very old ideas. Annu Rev Physiol 62, 51-77.

Nerbonne, J.M., 2000. Molecular basis of functional voltage-gated K+ channel diversity in the mammalian myocardium. J Physiol 525, 285-298.

Nerbonne, J.M., Kass, R.S., 2005. Molecular physiology of cardiac repolarization. Physiol Rev 85, 1205-1253.

Noble, D., Noble, P.J., 2006. Late sodium current in the pathophysiology of cardiovascular disease: consequences of sodium-calcium overload. Heart 92, 1-5.

Opie, L.H., 2004, Resting membrane potential, in: Heart Physiology: from cell to circulation, ed. Opie, L.H. (Lippincott Williams & Wilkins, Philadelphia) 77-78.

Orth, P.M.R., Hesketh, J.C., Mak, C.K.H., Yang, Y., Lin, S., Beatch, G.N., Ezrin, A.M., Fedida, D., 2006. RSD1235 blocks late INa and suppresses early afterdepolarizations and torsades de pointes induced by class III agents. Cardiovasc Res 70, 486-496.

Oudit, G.Y., Kassiri, Z., Sah, R., Ramirez, R.J., Zobel, C., Backx, P.H., 2001. The molecular physiology of the cardiac transient outward potassium current (Ito) in normal and diseased myocardium. J Mol Cell Cardiol 33, 851-872.

Pourrier, M., Schram, G., Nattel, S., 2003. Properties, expression and potential roles of cardiac K+ channel accessory subunits: MinK, MiRPs, KChIP, and KChAP. J Mem Biol 194, 141-152.

Puck, T.T., Cieciura, S.J., Robinson, A., 1958. Genetics of somatic mammalian cells: III. long-term cultivation of euploid cells from human and animal subjects. J Exp Med 108, 945-956.

Rasmusson, R.L., Morales, M.J., Wang, S., Liu, S., Campbell, D.L., Brahmajothi, M.V., Strauss, H.C., 1998. Inactivation of voltage-gated cardiac K+ channels. Circ Res 82, 739-750.

Roden, D.M., 2004. Drug-induced prolongation of the QT interval. N Engl J Med 350, 1013-1022.

Roden, D.M., B.F., H., 1985. Action potential prolongation and induction of abnormal automaticity by low quinidine concentrations in canine Purkinje fibers. Relationship to potassium and cycle length. Circ Res 56, 857-867.

Roden, D.M., Balser, J.R., George Jr, A.L., Anderson, M.E., 2002. Cardiac ion channels. Annu Rev Physiol 64, 431-475.

Rosati, B., Pan, Z., Lypen, S., Wang, H.-S., Cohen, I., Dixon, J.E., McKinnon, D., 2001. Regulation of KChIP2 potassium channel beta subunit gene expression underlies the gradient of transient outward current in canine and human ventricle. J Physiol 533, 119-125.

Sadja, R., Alagem, N., Reuveny, E., 2003. Gating of GIRK channels: details of an intricate, membrane-delimited signaling complex. Neuron 39, 9-12.

Salata, J.J., Jurkiewicz, N.K., Jow, B., Folander, K., Guinosso, P.J., Jr, Raynor, B., Swanson, R., Fermini, B., 1996. IK of rabbit ventricle is composed of two currents: evidence for IKs. Am J Physiol Heart Circ Physiol 271, H2477-2489.

Sanguinetti, M.C., Curran, M.E., Zou, A., Shen, J., Spector, P.S., Atkinson, D.L., Keating, M.T., 1996. Coassembly of KvLQT1 and minK (IsK) proteins to form cardiac IKs potassium channel. Nature 384, 80-83.

Sanguinetti, M.C., Jiang, C., Curren, M.E., Keating, M.T., 1995. A mechanistic link between an inherited and an acquired cardiac arrhythmia: hERG encodes the IKr potassium channel. Cell 81, 299-307.

Sasaki, Y., Ishii, K., Nunoki, K., Yamagishi, T., Taira, N., 1995. The voltage-dependent K+ channel (Kv1.5) cloned from rabbit heart and facilitation of inactivation of the delayed rectifier current by the rat beta subunit. FEBS Letters 372, 20-24.

Schreibmayer, W., Kazerani, H., Tritthart, H.A., 1987. A mechanistic interpretation of the action of toxin II from Anemonia sulcata on the cardiac sodium channel. Biochim Biophys Acta 901, 273-282.

Selzer, A., Wray, H.W., 1964. Quinidine syncope: paroxysmal ventricular fibrillation occurring during treatment of chronic atrial arrhythmias. Circulation 30, 17-26.

Shieh, B.H., Xia, Y., Sparkes, R.S., Klisak, I., Lusis, A.J., Nicoll, D.A., Philipson, K.D., 1992. Mapping of the gene for the cardiac sarcolemmal Na+-Ca2+ exchanger to human chromosome 2p21-p23. Genomics 12, 616-617.

Shiroshita-Takeshita, A., Brundel, B.J.J.M., Nattel, S., 2005. Atrial fibrillation: basic mechanisms, remodeling and triggers. J Intervent Card Electrophysiol 13, 181-193.

Sinclair, J., Pihl, J., Olofsson, J., Karlsson, M., Jardemark, K., Chiu, D.T., Orwar, O., 2002. A cell-based bar code reader for high-throughput screening of ion channel-ligand interactions. Anal Chem 74, 6133-6138.

Skryma, R., Prevarskaya, N., Vacher, P., Dufy, B., 1994. Voltage-dependent ionic conductances in Chinese hamster ovary cells. Am J Physiol Cell Physiol 267, C544-553.

Snyders, D.J., Knoth, K.M., Roberds, S.L., Tamkun, M.M., 1992. Time-, voltage-, and state-dependent block by quinidine of a cloned human cardiac potassium channel. Mol Pharmacol 41, 322-330.

Sontheimer, H., Ransom, C.B., 2002, Whole-cell patch-clamp recordings, in: *Patch-Clamp Analysis - Advanced Techniques*, eds. Walz, W., Boulton, A.A., Baker, G.B. (Humana press, Totowa, New Jersey) 35-67.

Striessnig, J., 1999. Pharmacology, structure and function of cardiac L-type Ca2+ channels. Cell Physiol Biochem 9, 242-269.

Studenik, C.R., Zhou, Z., January, C.T., 2001. Differences in action potential and early afterdepolarization properties in LQT2 and LQT3 models of long QT syndrome. Br J Pharmacol 132, 85-92.

Tamkun, M., Knoth, K., Walbridge, J., Kroemer, H., Roden, D., Glover, D., 1991. Molecular cloning and characterization of two voltage-gated K+ channel cDNAs from human ventricle. FASEB J 5, 331-337.

Tinel, N., Diochet, S., Borsotto, M., Lazdunski, M., Barhanin, J., 2000. KCNE2 confers background current characteristics to the cardiac KCNQ1 potassium channel. EMBO J 19, 6326-6330.

Trudeau, M., Warmke, J.W., Ganetzky, B., Robertson, G.A., 1995. hERG, a human inwared rectifier in the voltage-gated potassium channel family. Science 269, 92-95.

Tseng, G.-N., 2001. IKr: the hERG channel. J Mol Cell Cardiol 33, 835-849.

Undrovinas, A.I., Maltsev, V.A., Kyle, J.W., Silverman, N., Sabbah, H.N., 2002. Gating of the late Na+ channel in normal and failing human myocardium. J Mol Cell Cardiol 34, 1489.

van der Velden, H.M.W., van der Zee, L., Wijffels, M.C., van Leuven, C., Dorland, R., Vos, M.A., Jongsma, H.J., Allessie, M.A., 2000. Atrial fibrillation in the goat induces changes in monophasic action potential and mRNA expression of ion channels involved in repolarization. J Cardiovasc Electrophysiol 11, 1262-1269.

van Ginneken, A.C.G., Veldkamp, M.W., 1999. Implications of inhomogeneous distribution of IKs and IKr channels in ventricle with respect to effects of class III agents and beta-agonists. Cardiovasc Res 43, 20-22.

Vandenberg, J.I., Torres, A.M., Campbell, T.J., Kuchel, P.W., 2004. The hERG K+ channel: progress in understanding the molecular basis of its unusual gating kinetics. Eur Biophys J 33, 89-97.

Wang, Z., Feng, J., Shi, H., Pond, A., Nerbonne, J.M., Nattel, S., 1999. Potential molecular basis of different physiological properties of the transient outward K+ current in rabbit and human atrial myocytes. Circ Res 84, 551-561.

Wang, Z., Fermini, B., Nattel, S., 1993. Sustained depolarization-induced outward current in human atrial myocytes. Evidence for a novel delayed rectifier K+ current similar to Kv1.5 cloned channel currents. Circ Res 73, 1061-1076.

Warmke, J.W., Ganetzky, B., 1994. A family of potassium channel genes related to eag in Drosophila and mammals. Proc Natl Acad Sci U S A 91, 3438-3442.

Vassort, G., Talavera, K., Alvarez, J.L., 2006. Role of T-type Ca2+ channels in the heart. Cell Calcium 40, 205-220.

Vaughan-Williams, E.M., 1970, Classification of antiarrhythmic drugs 449-472.

Wettwer, E., Hala, O., Christ, T., Heubach, J.F., Dobrev, D., Knaut, M., Varro, A., Ravens, U., 2004. Role of IKur in controlling action potential shape and contractility in the human atrium: influence of chronic atrial fibrillation. Circulation 110, 2299-2306.

Wickman, K., Krapivinsky, G., Corey, S., Kennedy, M., Nemec, J., Medina, I., Clapham, D.E., 1999. Structure, G protein activation, and functinal relevance of the cardiac G protein-gated K+ channel, IKACh. Ann N Y Acad Sci 868, 386-398.

Wijffels, M.C.E.F., Dorland, R., Mast, F., Allessie, M.A., 2000. Widening of the excitable gap during pharmacological cardioversion of atrial fibrillation in the goat : effects of cibenzoline, hydroquinidine, flecainide, and d-sotalol. Circulation 102, 260-267.

Wijffels, M.C.E.F., Kirchhof, C.J.H.J., Dorland, R., Allessie, M.A., 1995. Atrial fibrillation begets atrial fibrillation : a study in awake chronically instrumented goats. Circulation 92, 1954-1968.

Volders, P.G.A., Stengl, M., van Opstal, J.M., Gerlach, U., Spatjens, R.L.H.M.G., Beekman, J.D.M., Sipido, K.R., Vos, M.A., 2003. Probing the contribution of IKs to canine ventricular repolarization: key role for beta-adrenergic receptor stimulation. Circulation 107, 2753-2760.

Volders, P.G.A., Vos, M.A., Szabo, B., Sipido, K.R., Maerieko de Groot, S.H., Gorgels, A.P.M., Wellens, H.J.J., Lazzara, R., 2000. Progress in the understanding of early afterdepolarisations and torsades de pointes: time to revise current concepts. Cardiovasc Res 46, 376-392.

Woodhull, A.M., 1973. Ionic blockade of sodium channels in nerve. J Gen Physiol 61, 687-708.

Wu, Y., Carlsson, L., Liu, T., Kowey, P.R., Yan, G.-X., 2005. Assessment of the proarrhythmic potential of the novel antiarrhythmic agent AZD7009 and dofetilide in experimental models of Torsades de Pointes. J Cardiovasc Electrophysiol 16, 898-904.

Wymore, R.S., Gintant, G.A., Wymore, R.T., Dixon, J.E., McKinnon, D., Cohen, I.S., 1997. Tissue and species distribution of mRNA for the IKr-like K+ channel, erg. Circ Res 80, 261-268.

Yamada, M., 2002. The role of muscarinic K+ channels in the negative chronotropic effect of a muscarinic agonist. J Pharmacol Exp Ther 300, 681-687.

Yamada, M., Inanobe, A., Kurachi, Y., 1998. G protein regulation of potassium ion channels. Pharmacol Rev 50, 723-757.

Yan, G.-X., Antzelevitch, C., 1998. Cellular basis for the normal T wave and the electrocardiographic manifestations of the long-QT syndrome. Circulation 98, 1928-1936.

Yan, G.-X., Lankipalli, R.S., Kowey, P.R., 2002. Current concepts in the management of long QT syndrome. Exp Opin Ther Pat 12, 633-643.

Yan, G.-X., Wu, Y., Liu, T., Wang, J., Marinchak, R.A., Kowey, P.R., 2001. Phase 2 early afterdepolarization as a trigger of polymorphic ventricular tachycardia in acquired long-QT syndrome : direct evidence from intracellular recordings in the intact left ventricular wall. Circulation 103, 2851-2856.

Yang, T., Kupershmidt, S., Roden, D.M., 1995. Anti-minK antisense decreases the amplitude of the rapidly activating cardiac delayed rectifier K+ current. Circ Res 77, 1246-1253.

Yu, H., Wu, J., Potapova, I., Wymore, R.T., Holmes, B., Zuckerman, J., Pan, Z., Wang, H., Shi, W., Robinson, R.B., El-Maghrabi, M.R., Benjamin, W., Dixon, J., McKinnon, D., Cohen, I.S., Wymore, R., 2001. MinK-related peptide 1 : a beta subunit for the HCN ion channel subunit family enhances expression and speeds activation. Circ Res 88, 84-87.

Yue, L., Wang, Z., Rindt, H., Nattel, S., 2000. Molecular evidence for a role of Shaw (Kv3) potassium channel subunits in potassium currents of dog atrium. J Physiol 527, 467-478.

Zeng, J., Rudy, Y., 1995. Early afterdepolarisations in cardiac myocytes: mechanism and rate dependence. Biophys J 68, 949-964.

Zhang, M., Jiang, M., Tseng, G.-N., 2001. MinK-related peptide 1 associates with Kv4.2 and modulates its gating function : potential role as beta subunit of cardiac transient outward channel? Circ Res 88, 1012-1019.

Zobel, C., Cho, H.C., Nguyen, T.-T., Pekhletski, R., Diaz, R.J., Wilson, G.J., Backx, P.H., 2003. Molecular dissection of the inward rectifier potassium current (IK1) in rabbit cardiomyocytes: evidence for heteromeric co-assembly of Kir2.1 and Kir2.2. J Physiol 550, 365-372.

Zygmunt, A.C., Eddlestone, G.T., Thomas, G.P., Nesterenko, V.V., Antzelevitch, C., 2001. Larger late sodium conductance in M cells contributes to electrical heterogeneity in canine ventricle. Am J Physiol Heart Circ Physiol 281, H689-697.

Ördög, B., Brutyo, E., Puskas, L.G., Papp, J.G., Varro, A., Szabad, J., Boldogkoi, Z., 2006. Gene expression profiling of human cardiac potassium and sodium channels. Int J Cardiol 111, 393.